ELSEVIER

Contents lists available at ScienceDirect

Metabolic Engineering

journal homepage: www.elsevier.com/locate/meteng





Metabolic engineering of *Corynebacterium glutamicum* for increased *cis, cis-*muconate production from plant-derived *p*-hydroxycinnamates via deregulated pathway flux and increased CoA intermediate availability

Fabia Weiland, Kyoyoung Seo, Franka Janz, Marius Grad, Lea Geldmacher, Michael Kohlstedt, Judith Becker, Christoph Wittmann *©

Institute of Systems Biotechnology, Saarland University, Saarbrücken, Germany

ARTICLE INFO

Keywords:

 $Coryne bacterium\ glutamicum$

 $p ext{-Hydroxycinnamates}$

Cinnamates Ferulate

p-Coumarate

Caffeate

Cinnamate

3,4-Dimethoxycinnamate

4-Methoxycinnamate

AroY PhdR

mCherry

Cis. cis-Muconic acid

Biobased Biosensor

Lignin

13C tracer

Metabolomics Acetyl-CoA

GlxR

ABSTRACT

Lignocellulosic biomass represents a promising renewable feedstock for sustainable biochemical production, with p-hydroxycinnamates emerging as key aromatic building blocks derived from agricultural residues and grassy plants. C. glutamicum has recently been engineered to produce cis, cis-muconate (MA), a high-value platform chemical used in biobased plastics, resins, and specialty chemicals. However, unlike other aromatics, the metabolism of the p-hydroxycinnamates p-coumarate, ferulate, and caffeate in MA-producing C. glutamicum is inefficient, limiting MA production performance. Here, we discovered that p-hydroxycinnamate metabolism, encoded by the phd operon, is repressed by the local repressor PhdR under glucose-rich conditions, while the global regulator GlxR activates the pathway in the absence of glucose. The deregulated C. glutamicum MA-10 lacking phdR exhibited an up to 98-fold increase in the conversion of p-coumarate, ferulate, and aromatic mixtures derived from plant waste into MA. Transcriptomic and metabolomic analyses revealed strong induction of the phd operon in strain MA-10 and a marked increase in intracellular aromatic CoA-esters and acetyl-CoA, indicating enhanced flux through the p-hydroxycinnamate degradation pathway. ¹³C-tracer studies demonstrated a substantial contribution of aromatic side-chain carbon to central metabolic pathways, supporting biomass formation and enabling MA production even in the absence of sugars. Additionally, MA-10 showed broadened substrate flexibility, degrading cinnamate into MA and methoxylated cinnamates into valuable benzoate derivatives. The strain also successfully converted aromatics from real straw lignin hydrolysates into MA. Our findings reveal the potential of targeted regulatory engineering to optimize C. glutamicum for lignin valorization. The newly developed strain MA-10 provides a robust platform for the biobased production of MA from lignocellulosic feedstocks, paving the way for sustainable and economically viable biorefinery processes.

1. Introduction

Grassy plants, including energy crops such as *miscanthus* and switchgrass, as well as residues from staple agricultural species such as corn, wheat, and rice, represent particularly attractive feedstocks for lignocellulosic biorefineries because of their global abundance (Andrade et al., 2021; Bichot et al., 2018). According to the Food and Agriculture Organization (FAO), global cereal production in 2024/25 is projected to be approximately 2.842 million tons, generating several hundred million tons of agricultural residues (e.g., wheat straw, rice straw, corn stover) on an annual basis (Gonçalves et al., 2020). Open field burning, which is commonly applied to remove these residues, causes severe

environmental problems, including air pollution, a risk of wildfires, soil deprivation and the emission of greenhouse gases (FAO, 2022).

A defining characteristic of grassy plants is their complex cell wall structure, which is particularly rich in *p*-hydroxycinnamates, primarily *p*-coumarate and ferulate. These hydroxycinnamates play crucial roles in reinforcing the grass cell wall by promoting crosslinking and increasing mechanical strength (Hatfield et al., 2017; Peracchi et al., 2024; Zhang et al., 2022). Importantly, they can be efficiently extracted via alkaline depolymerization (Jiang et al., 2016; Karp et al., 2016; Ou et al., 2009; Rodriguez et al., 2017; Torre et al., 2008), making them readily accessible for microbial conversion into value-added biochemicals using metabolically engineered bacteria (Bugg et al., 2021; Liu et al., 2024;

E-mail address: christoph.wittmann@uni-saarland.de (C. Wittmann).

https://doi.org/10.1016/j.ymben.2025.08.004

^{*} Corresponding author.

Weiland et al., 2022).

Although caffeate is typically less abundant than *p*-coumarate and ferulate in agricultural residues, notable exceptions exist, making the compound interesting too. In rice straw, caffeate is the dominant phenolic compound (Karimi et al., 2014), and it is also present in significant amounts in agro-industrial byproducts like soybean meal (Oskoueian et al., 2011), spent coffee grounds (Angeloni et al., 2020), and sorghum straw (Oian et al., 2024).

A promising host for lignin valorization is *Corynebacterium gluta-micum*, a well-established industrial microbe traditionally used for the production of amino acids and other metabolites from primary sugars such as glucose, fructose, and sucrose (Becker and Wittmann, 2012). Notably, *C. glutamicum* has been leveraged to synthesize more than 90 different products from such carbon sources (Becker et al., 2018b).

Recent advances have expanded its substrate range to produce cis, cis-muconate (MA) from lignin-derived aromatic precursors (Li et al., 2024). Importantly, MA is a highly versatile platform chemical that serves as the starting point for the synthesis of adipic acid and terephthalic acid, paving the way for the production of different biobased plastics (Kohlstedt et al., 2018, 2022). Microbiologically produced MA is promising and sustainable alternative to its petrochemical-derived counterparts (Corona et al., 2018; Mokwatlo et al., 2024; van Duuren et al., 2020). A pioneering study engineered C. glutamicum for MA production from catechol and catechol-rich lignin hydrolysates obtained via hydrothermal depolymerization (Becker et al., 2018a). Building on this foundation, we further advanced the metabolic engineering of C. glutamicum to enable MA production from vanillin and vanillate, which are key aromatic compounds derived from the alkaline oxidation of softwood lignin (Weiland et al., 2023) (Fig. 1).

Here, we aimed to enhance the valorization of *p*-hydroxycinnamates into MA. The native metabolism of p-coumarate, ferulate, and caffeate in microbes is initiated by a common enzymatic pathway encoded by the phd (phenylpropanoid degradation) operon (Kallscheuer et al., 2016) (Fig. 1). At the beginning of this study, we identified carbon catabolite repression (CCR) as a major barrier to phd operon activation in the presence of glucose, the primary growth substrate, thereby restricting MA production from aromatics. We employed carefully designed sensor strains to systematically dissect the regulation of this pathway, and the results provided quantitative insights into glucose-mediated repression and its interaction with a diverse range of hydroxycinnamates and cinnamates. This analysis revealed a critical metabolic bottleneck that hindered efficient aromatic utilization. We deleted phdR in the previously engineered MA producer C. glutamicum MA-6A (Weiland et al., 2023), generating strain MA-10 to overcome this limitation. The mutant exhibited a strong increase in the degradation of p-coumarate, ferulate, and aromatic mixtures. Integrated metabolomic, transcriptomic, and ¹³C tracer analyses revealed that phdR deletion alleviated carbon catabolite repression, enabling strain MA-10 to co-metabolize glucose and p-hydroxycinnamates with enhanced MA production. This deregulation led to increased intracellular CoA thioesters and acetyl-CoA, indicating a strong link between aromatic catabolism and central metabolism. Isotopic labeling showed side-chain carbons from p-coumarate contributed to biomass via acetyl-CoA through the TCA cycle, glyoxylate shunt, and gluconeogenesis. Strain MA-10 also produced MA from p-coumarate without glucose, showed an expanded substrate range towards p-methoxylated cinnamates and converted straw lignin hydrolysates into MA, supporting its potential for lignocellulosic aromatic valorization.

2. Materials and methods

2.1. Microorganisms and plasmids

C. glutamicum ATCC 13032 (DSM, 20300) (Becker et al., 2011) and C. glutamicum MA-6A (Weiland et al., 2023) were derived from previous work. For plasmid amplification, Escherichia coli DH10B (Life GmbH,

Darmstadt, Germany) and NM522 (Invitrogen, Carlsbad, CA, USA) strains were used. NM522 carries the plasmid pTC to ensure *C. glutamicum*-specific DNA methylation (Kind et al., 2010). All the strains were preserved as cryostocks in 30 % glycerol at -80 °C. Genome-based deletions were performed using the integrative vector pClik int *sacB* (Becker et al., 2005), whereas the episomal vector pClik 5a MCS was used to express mCherry-reporter constructs, as described previously (Pauli et al., 2023). A complete list of the strains and plasmids used in this study is provided in Table 1.

2.2. Genetic engineering

Strains, plasmids, and primers were designed using SnapGene (GSL Biotech LLC, Insightful Science, Chicago, IL, USA). Plasmids for stable genetic modifications and reporter assays were constructed as previously described (Pauli et al., 2023; Weiland et al., 2023). Briefly, the integrative vector pClik int SacB or the episomal vector pClik 5a MCS was linearized using BamHI (FastDigest, Thermo Fisher Scientific, Waltham, MA, USA) with the addition of FastAP Thermosensitive Alkaline Phosphatase (Thermo Fisher Scientific), DNA fragments were amplified by PCR (Phusion High-Fidelity PCR Master Mix with GC Buffer, Thermo Fisher Scientific) using construct-specific primers (Table S1, Supplementary File 1), purified (Wizard SV Gel & PCR Clean-Up System, Promega, Mannheim, Germany), and assembled with the linearized vector (Rohles et al., 2016). The plasmids were initially transformed into E. coli DH10B and were subsequently isolated from the correct clones using the innuPREP Plasmid Mini Kit 2.0 (IST Innuscreen GmbH, Berlin, Germany). Integrative plasmids were additionally transformed into E. coli NM522+pTC to ensure C. glutamicum-specific methylation. Heat-shock transformation was used for E. coli, whereas electroporation was applied for C. glutamicum. Defined mutant strains carrying integrative constructs were generated as described previously (Becker et al., 2010; Kind et al., 2010; Rohles et al., 2022). All plasmids and strains were validated by PCR and sequencing (Azenta Life Sciences, Genewiz Germany, Leipzig, Germany).

2.3. Alkaline depolymerization of straw lignin

BioligninTM, a wheat straw-based lignin, was kindly provided by CIMV (Compagnie Industrielle de la Matière Végétale) from their organosolv refining process (Cachet et al., 2014). It was depolymerized using a base-catalyzed process (Katahira et al., 2016; Rodriguez et al., 2017). Lignin (7.5 g) was suspended in 250 mL of 0.5 M sodium hydroxide solution. The suspension was purged three times with nitrogen while stirring at 400 rpm to ensure an inert atmosphere. Depolymerization was carried out at 120 °C for 30 min and then rapidly quenched in an ice bath. The resulting hydrolysate was neutralized with 6 M HCl. Insoluble residues were removed by centrifugation (5000×g, 5 min, room temperature) followed by filtration (0.45 μ m). The aromatic monomer content of the alkaline lignin hydrolysate was analyzed by high-performance liquid chromatography (HPLC) and confirmed by GC-MS using commercially available standards (see below).

2.4. Media

For the routine cultivation of *E. coli* and *C. glutamicum*, complex medium (37 g L $^{-1}$ brain heart infusion, BHI, Becton Dickinson, Franklin Lakes, NJ, USA) was used. For solid media, the complex medium was supplemented with 20 g L $^{-1}$ BD Difco agar (Becton Dickinson). For *C. glutamicum*, minimal medium was prepared that contained the following components per liter: 11 g of glucose monohydrate, 15 g of (NH₄)₂SO₄, 1 g of NaCl, 0.2 g of MgSO₄*7H₂O, 0.055 g of CaCl₂, 2 mg of FeCl₃*6H₂O, 2 mg of MnSO₄*H₂O, 0.5 mg of ZnSO₄*H₂O, 0.2 mg of CuCl₂*2H₂O, 0.2 mg of Na₂B₄O₇*10H₂O, 0.1 mg of (NH₄)₆Mo₇O₂₄*4H₂O, 20 mg of FeSO₄*7H₂O, 1 mg of thiamin-HCl, 1 mg of Ca-pantothenate, 0.5 mg of biotin, 30 mg of 3,4-dihydroxybenzoate

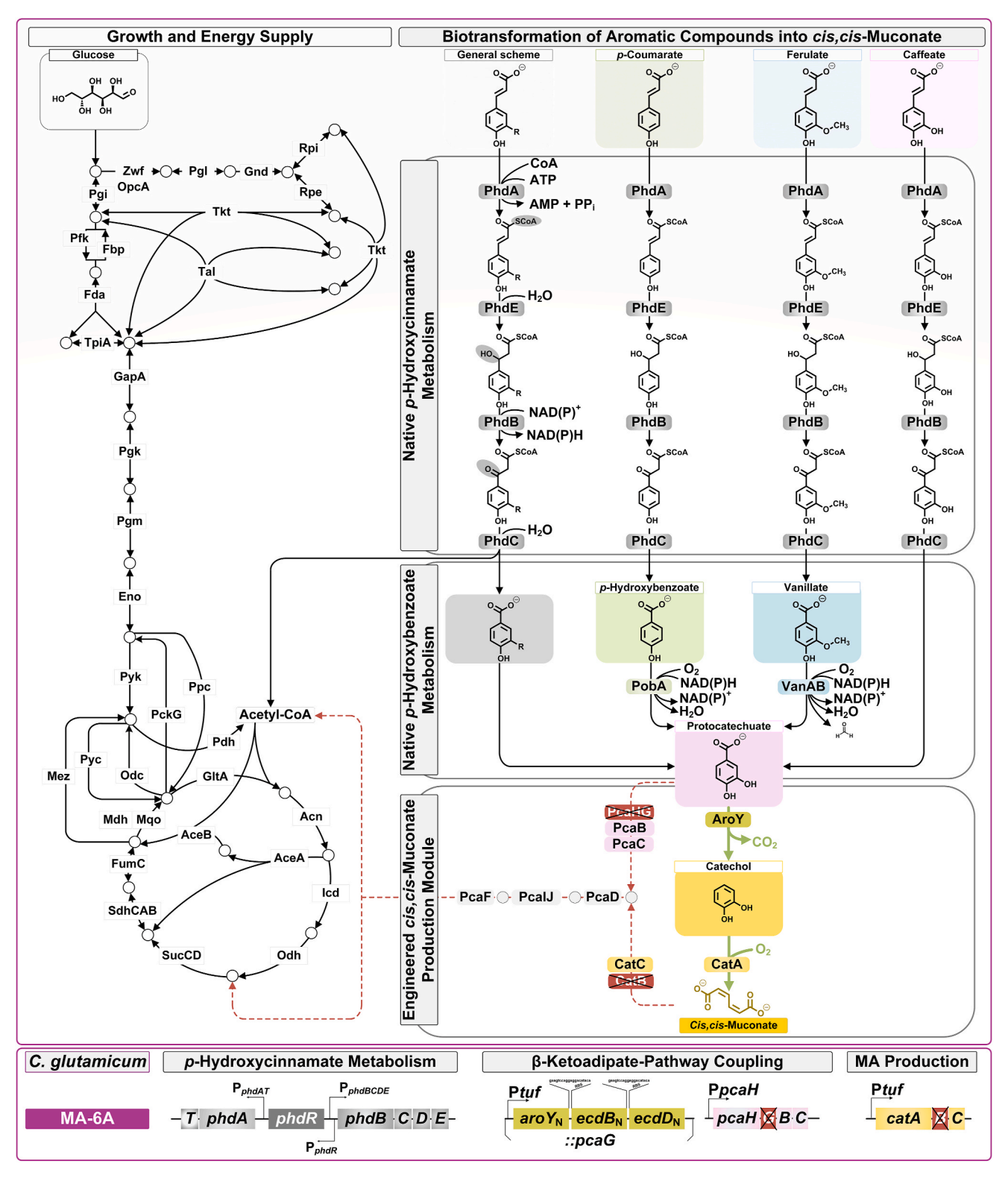


Fig. 1. Metabolic pathways of *p*-hydroxycinnamate-based *cis*, *cis*-muconate (MA) production in the metabolically engineered *C. glutamicum* strain MA-6A. The *phd* pathway breaks down *p*-coumarate, ferulate, and caffeate and yields the corresponding pathway intermediates vanillate, *p*-hydroxybenzoate, and protocatechuate. The *phd* operon consists of seven genes: (i) *phdA*–*phdE*, encoding enzymes involved in the β-oxidation of *p*-hydroxycinnamates; (ii) *phdT*, encoding a putative transporter; and (iii) *phdR*, a transcriptional repressor regulating the *phd* gene cluster (Kallscheuer et al., 2016). The metabolism of *p*-hydroxycinnamates is initiated by its conversion into the corresponding CoA ester, which is catalyzed by PhdA, followed by a three-step side-chain cleavage pathway. The resulting *p*-hydroxybenzoate analogs are subsequently funneled into the central intermediate protocatechuate in an oxygen-dependent manner (Weiland et al., 2022). In the metabolically engineered strain MA-6A, MA production is enabled by the deletion of *catB*, the overexpression of *catA*, and the rerouting of protocatechuate metabolism toward MA biosynthesis. This process is achieved by introducing the heterologous protocatechuate decarboxylase gene *aroY*, as well as *ecdB* and *ecdD* from *Enterobacter cloacae*, into the *pcaG* locus (Weiland et al., 2023). Enzyme annotations for central carbon and aromatic compound metabolism are provided in Supplementary File 1. Overexpressed enzymatic reactions are indicated by thick green lines; deleted enzymatic reactions are shown as red dashed lines.

Table 1
Strains and plasmids.

Strains/Plasmids	Description	Reference
E. coli DH10B	Vector amplification and maintenance	Korneli et al. (2013)
NM522 + pTC	Vector amplification and methylation	Kind et al. (2010)
BL21 (DE3)	High-level expression of recombinant proteins	Seo et al. (2023)
p28phdA	Derivative of <i>E. coli</i> BL21 (DE3) harboring the p28phdA plasmid	This work
p28phdE	Derivative of <i>E. coli</i> BL21 (DE3) harboring the p28phdE plasmid	This work
p28ferA	Derivative of <i>E. coli</i> BL21 (DE3) harboring the p28ferA plasmid	This work
C. glutamicum DSM 20300	Wildtype	Becker et al.
MA-2	Wildtype, deletion of catB (NCgl2318),	(2018a) Becker et al.
	overexpression of <i>catA</i> ($NCgl2319$) under the control of P_{tuf} ($NCgl0480$)	(2018a)
MA-6A	MA-2, integration of <i>aroY</i> (<i>Ecl_01944</i>), <i>ecdB</i> (<i>Ecl_04083</i>), and <i>ecdD</i> (<i>Ecl_04081</i>) from	Weiland et al. (2023)
	E. cloacae under the control of P _{tuf} in the pcaG locus (NCgl2314)	
P _{phdAT} mCherry	Wildtype, episomal <i>mCherry</i> expression (AFV60003; pSEVA247R) under the control	This work
P _{phdBCDE} mCherry	of <i>P_{phdAT}</i> (<i>NCgl0278-NCgl0279</i>) Wildtype, episomal <i>mCherry</i> expression (AFV60003; pSEVA247R) under the control	This work
P _{phdAT} mCherry	of $P_{phdBCDE}$ (NCgl0281- NCgl0284) Wildtype, episomal mCherry expression under the control of P_{phdAT}^{mut}	This work
P ^{mut} _{phdBCDE} mCherry	Wildtype, episomal $mCherry$ expression under the control of $P_{phdBCDE}^{mut}$	This work
MA-10	MA-6A, deletion of phdR (NCgl0280)	This work
MA-11	MA-10, deletion of vanAB (NCgl2300- NCgl2301)	This work
Plasmids		
pTC	Vector for the DNA methyltransferase of C. glutamicum with an origin of replication	Kind et al. (2010)
pClik int SacB	for E . $coli$ and tet^R as the selection marker Integrative vector with a MCS, an ORI for E . $coli$, and kan^R and $sacB$ as selection	Kind et al. (2010)
pClik 5a MCS α	markers Episomal vector with a MCS, an ORI for E. coli and C. glutamicum, and kan ^R as the	Kind et al. (2010)
pClik int SacB	selection marker Deletion of <i>phdR</i>	This work
ΔphdR pClik 5a MCS α	Expression of <i>mCherry</i> under the control of	This work
P _{phdAT} mCherry pClik 5a MCS α P _{phdBCDE}	P_{phdAT} Expression of <i>mCherry</i> under the control of $P_{phdBCDE}$	This work
mCherry pClik 5a MCS α P ^{mut} _{phdAT} mCherry	Expression of <i>mCherry</i> under the control of P_{phdAT}^{mut}	This work
pClik 5a MCS α $P_{phdBCDE}^{mut}$	Expression of <i>mCherry</i> under the control of $P_{phdBCDE}^{mut}$	This work
mCherry pClik int SacB ΔναnAB	Deletion of vanAB	This work
pET-28a	Vector for protein expression	Invitrogen
p28phdA	pET-28a-derived protein expression vector for phdA (NCgl0279) from C. glutamicum DSM 20300	This work
p28phdE	pET-28a-derived protein expression vector for phdE (NCgl0284) from C. glutamicum DSM 20300	This work
p28ferA	pET-28a-derived protein expression vector for the ferA (SARO_RS03365) gene of N. aromaticivorans DSM 12444	This work

(or 100 mg L⁻¹ EDTA), and 200 mM potassium phosphate buffer (pH 7.8) (Rohles et al., 2022). For isotopic tracer studies, normal glucose was replaced with 99 % [U-13C₆] glucose (Cambridge Isotope Laboratories, Inc., Tewksbury, MA, USA). For the conversion experiments, the medium was supplemented with aromatic compounds from filter-sterilized stock solutions (10-50 mM in water, dissolved in 10 M NaOH). The tested substrates included p-coumarate, ferulate, caffeate, p-methoxvcinnamate, 3,4-dimethoxycinnamate, cinnamate, sinapinate, p-hydroxybenzoate, protocatechuate, and benzoate. In an alternative approach, straw lignin-derived hydrolysate was added at varying concentrations of 20 %, 40 %, and 60 % (v/v). Additionally, a sugar-free conversion condition was tested by omitting glucose from the medium and supplying p-coumarate as the sole carbon source to evaluate the potential of utilizing aromatic compounds independently of sugars. When needed, antibiotics (50 µg mL⁻¹ kanamycin and 12.5 µg mL⁻¹ tetracycline) were added for plasmid maintenance (Pauli et al., 2023).

2.5. Batch cultivation in shake flasks

Cultivations were performed as described previously (Weiland et al., 2023) using a three-step process: two successive precultures and a main culture. All cultures were grown in baffled shake flasks with a 10 % filling volume on an orbital shaker at 30 °C and 230 rpm (Multitron, Infors-HT, Bottmingen, Switzerland; shaking diameter: 5 cm, 80 % humidity control). The first preculture was initiated by inoculating 10 mL of BHI complex medium with a single colony from a BHI-agar plate, which had been preincubated at 30 °C for 48 h. For the second preculture, the cells were harvested by centrifugation ($6000 \times g$, 4 min, RT) and transferred to 25 mL of minimal medium. After an overnight incubation, the cells were collected and prepared for the main culture. In the main culture, cells from the second preculture were inoculated into 25 mL of minimal medium supplemented with the aromatic biotransformation substrate. All the experiments were conducted in biological triplicates to ensure reproducibility.

2.6. Screening in miniaturized bioreactors

Using the same preculture procedure as described above, the main cultures were conducted in a microbioreactor (BioLector, Beckman Coulter GmbH, Baesweiler, Germany). Cultivations were performed in 48-well FlowerPlates (MTP-48 B, Beckman Coulter GmbH) for 24 h in 1 mL of medium at 30 °C, 1300 rpm, and 85 % relative humidity (Becker et al., 2018a). Additionally, an online fluorescence measurement of the mCherry reporter protein was performed using a wavelength-specific filter (excitation: 580 nm, emission: 610 nm) (Kohlstedt et al., 2018). All the experiments were conducted in biological triplicates.

2.7. Quantification of the cell concentration, substrates, and products

The cell concentration was determined photometrically by measuring the optical density at 660 nm (OD₆₆₀). The cell dry mass (CDM) was calculated from the measured OD₆₆₀ using a previously determined correlation factor (CDM [g/L] = $0.32 \times OD_{660}$) (Rohles et al., 2016). The concentrations of glucose and various aromatic compounds were quantified by HPLC, as previously described (Weiland et al., 2023). For the analysis of lignin hydrolysate samples, which present a more complex matrix, the HPLC gradient was modified as follows: 0-24.0 min, 99-67 % solvent A; 24.0-27.0 min, 67-0 % A; 27.0-30.0 min, 0 % A; 30.0-31.5 min, 0-99 % A; and 31.5-36.5 min, 99 % A. For the quantification of aromatics and novel biotransformation products derived from p-hydroxycinnamic acid metabolism, specific wavelengths were used. p-Anisic acid was measured at 200 nm, while protocatechuic acid, p-hydroxybenzoic acid and catechol were detected at 210 nm. Vanillic acid, veratric acid, and isovanillic acid were quantified at 220 nm, and benzoic acid was quantified at 230 nm. Cis, cis-muconic acid and trans-cinnamic acid were measured at 260 nm.

p-Coumaric acid, ferulic acid, and 4-methoxycinnamic acid were detected at 310 nm, while caffeic acid, 3,4-dimethoxycinnamic acid, and sinapinic acid were quantified at 325 nm.

2.8. Enzymatic synthesis and purification of aromatic CoA-ester standards

The enzymatic synthesis of commercially unavailable thioester standards was based on previous work (Seo et al., 2023). The backbone of the pET-28a expression vector (Invitrogen) was digested with Fast-Digest NcoI and XhoI (Thermo Fisher Scientific) to obtain aromatic CoA thioesters, including p-coumaroyl-CoA and 3-hydroxy-p-coumaroyl-CoA. The two genes, phdA, encoding acyl-CoA ligase, and phdE, encoding enoyl-CoA hydratase, were amplified from C. glutamicum ATCC 13032 using Phusion High-Fidelity PCR Master Mix with HF Buffer (Thermo Fisher Scientific). Additionally, ferA, encoding an acetate-CoA ligase (Cecil et al., 2018), was amplified from the genomic DNA of Novosphingobium aromaticivorans DSM 12444 (DSMZ, German Collection of Microorganisms and Cell Cultures GmbH, Braunschweig, Germany) using Phusion High-Fidelity PCR Master Mix with GC Buffer (Thermo Fisher Scientific). The primers used for the amplification of the target genes can be found in Table S2 (Supplementary File 1). Each gene was subsequently assembled into the linearized pET-28a vector via Gibson assembly, followed by transformation into E. coli BL21 (DE3) (Thermo Fisher Scientific) through heat shock and verification by sequencing. E. coli BL21 (DE3) cells harboring the respective pET-28a-derived plasmids were plated on LB agar supplemented with kanamycin and incubated overnight at 37 °C. A single colony was used as the inoculum in 10 mL of LB medium containing kanamycin in a 100 mL shaker flask, followed by an incubation at 37 °C and 160 rpm on an orbital shaker. The entire culture was subsequently transferred into 300 mL of Terrific Broth (TB) medium supplemented with kanamycin in a 1 L shaker flask and incubated at 28 °C with shaking. Protein expression was induced at an OD_{600} of 0.7 by the addition of 0.5 mM isopropyl β-D-1-thiogalactopyranoside (IPTG), followed by continued incubation overnight at 28 °C. Then, the cells were harvested by centrifugation $(5000 \times g, 10 \text{ min}, 4 \,^{\circ}\text{C})$, and the pellet was resuspended in buffer A (450 mM NaCl, 50 mM HEPES-KOH, 15 % (v/v) glycerol, pH 7.6) at a 2:1 (v/w) ratio. After cell disruption by sonication, the cell debris was removed by centrifugation (10,000×g, 45 min, 4 °C), after which the resulting supernatant was filtered (0.45 µm) and applied onto Ni-NTA agarose beads (Protino, Macherey-Nagel) for protein purification. The column was washed with 10 mL of buffer C (350 mM NaCl, 50 mM HEPES, 15 % (v/v) glycerol, pH 7.8) to remove nonspecifically bound proteins. The target protein was then eluted with buffer B (20 mM NaCl, 50 mM HEPES, 10 % glycerol, and 500 mM imidazole, pH 7.6).

Enzymatic synthesis was performed using specific CoA ligases and β -oxidation enzymes to obtain pure reference standards for p-coumaroyl-CoA and 3-hydroxy-p-coumaroyl-CoA. For the synthesis of p-coumaroyl-CoA, the resulting enzymes, acyl-CoA ligase (PhdA) or acetate-CoA ligase (FerA), were used. Additionally, 3-hydroxy-p-coumaroyl-CoA was synthesized using both the PhdA and PhdE enzymes. Aromatic precursors were prepared at a final concentration of 6.52 mM and dissolved in deionized water. These solutions were mixed with CoA trilithium salt (2.17 mM, Sigma–Aldrich) and ATP (6.52 mM final concentration). The reaction mixture also contained 20 mM MgCl $_2$, 50 mM KHCO $_3$, and 50 mM HEPES buffer (pH 7.5). The enzymatic reaction was initiated by the addition of 10 μ M of the respective enzyme and incubated for 1 h (30 °C, 230 rpm). After the incubation, the reaction was quenched by adding 10 % (v/v) formic acid, followed by centrifugation (4500×g, 20 min, 25 °C) to remove debris.

Following synthesis, the CoA thioesters were purified using an Agilent 1260 Infinity prep-LC system equipped with a Gemini 10 μm NX-C18 reverse-phase column (100 \times 21.2 mm, AXIA Packed, Phenomenex, Aschaffenburg, Germany). A gradient of solvent A (25 mM ammonium formate, pH 5.5) and solvent B (methanol) was applied at a

flow rate of 1 mL per minute. The gradient program consisted of an increase from 5 % to 50 % B over 15 min, followed by a 2-min wash with 95 % B, and then re-equilibration for 2 min at 5 % B. Fractions containing purified CoA thioesters were pooled, flash-frozen in liquid nitrogen, lyophilized, and stored at $-20~^{\circ}\text{C}$. The concentrations of the purified CoA thioesters were determined photometrically using established extinction coefficients. The extinction coefficient for p-coumaroyl-CoA was $\epsilon_{333}=21~\text{mM}^{-1}~\text{cm}^{-1}$ (Rautengarten et al., 2010). For the purification of 3-hydroxy-p-coumaroyl-CoA, all the fractions exhibiting signals at 260 nm (based on the adenine moiety) were collected. The presence of the desired analyte was confirmed via LC–MS analysis ([M+H] $^+=932.2$).

2.9. LC-MS/MS analysis of CoA thioesters

The cells from a 50 mL culture grown in chemically defined minimal medium were harvested at an OD $_{660}=4$ by centrifugation (6000×g, 4 min, 4 °C) (Gläser et al., 2020). For efficient quenching, the resulting pellet was resuspended in 25 mL of 25 mM formic acid in 95 % acetonitrile (-20 °C), mixed thoroughly, and incubated on ice for 10 min. The suspension was centrifuged ($10,000\times 10$ min, 4 °C) to remove the cell debris, and the supernatant was transferred into 5 mL of supercooled deionized water. After the pellet was washed once with an additional 5 mL of supercooled deionized water, both supernatants were combined. The final extract was immediately frozen in liquid nitrogen and lyophilized. For further analysis, the lyophilized samples were resuspended in 700 µL of resuspension buffer (25 mM ammonium formate, pH 5.6, and 2 % methanol, 4 °C) and centrifuged (13,000×g, 4 min, 4 °C). The resulting supernatants were used for further analysis.

LC-ESI-MS/MS was performed using an Agilent Infinity 1290 LC system coupled to an AB Sciex QTrap 6500 mass spectrometer to analyze the intracellular and synthetic CoA thioesters (Gläser et al., 2020, 2021). Chromatographic separation was achieved using a Kinetex 2.6 µm XB-C18 column (100 \times 2.1 mm, Phenomenex) maintained at 40 $^{\circ}$ C and the following gradient of eluent A (50 mM formic acid, adjusted to pH 8.1 with 25 % ammonium hydroxide) and eluent B (methanol): 0 min, 100 % eluent A; 3 min, 85 % eluent A; 8 min, 75 % eluent A; and 10 min, 0 % eluent A. Afterward, the column was rinsed for 1 min and re-equilibrated for 2 min. The flow rate was maintained at 300 µL per minute. Mass spectrometry was performed in positive ion mode ([M+H]+). The ion spray voltage was set to 4.5 kV, with a source temperature of 400 °C. Additional settings included a curtain gas pressure of 35 psi, an ion source gas pressure of 60 psi, and an entrance potential of 10 V. The collision gas was set to medium flow. Structural confirmation of the purified hydroxy-aromatic CoA thioesters was performed using LC-MS/MS, with expected masses of 914.2 ([M+H]⁺) for p-coumaroyl-CoA, 932.3 ([M+H]⁺) for 3-hydroxy-p-coumaroyl-CoA, and 930.1 ([M+H]⁺) for 3-oxo-p-coumaroyl-CoA. Multiple reaction monitoring (MRM) was used to detect specific CoA thioesters. The best-suited MRM transitions and the elution times of p-coumaroyl-CoA (m/z 914.1 \rightarrow 407.2) and 3-hydroxy-p-coumaroyl-CoA (m/z 932.1 \rightarrow 425.2) were determined from analysis of the pure compounds. In contrast, 3-oxo-p-coumaroyl-CoA could not be obtained synthetically; thus, the MRM transition used was based on the expected masses (m/z) $930.1 \rightarrow 423.1$), and the elution time was inferred from that of related compounds. The analysis of acetyl-CoA was based on previous methods (Gläser et al., 2020; Jovanovic Gasovic et al., 2023). Absolute quantification of aromatic CoA-thioesters was not feasible due to the lack of commercially available synthetic standards required for calibration using the MIRACLE approach, the current gold standard for accurate CoA-thioester quantification in microbes (Beganovic et al., 2023; Dietrich et al., 2023; Dolan et al., 2022; Jovanovic Gasovic et al., 2023; Kuhl et al., 2020; Seo et al., 2023). Nevertheless, relative quantification of these CoA-thioester levels was successfully performed, providing consistent and biologically meaningful data that support the study's conclusions.

2.10. Identification of aromatic pathway intermediates by GC-MS

The structures of aromatic pathway intermediates were identified using gas chromatography-mass spectrometry (GC-MS) according to previously established protocols (Weiland et al., 2023). Culture supernatants (50 µL) were dried under a gentle nitrogen stream, and the obtained solids were dissolved in 50 µL of dimethylformamide (0.1 % pyridine). Lignin hydrolysates (500 µL) were acidified with 6 M HCl and dried under a nitrogen stream. The resulting solids were resuspended in $250~\mu L$ of pure ethanol, and the ethanol phase - containing the target analytes - was collected and evaporated to dryness under nitrogen. The final residue was dissolved in $50 \mu L$ of dimethylformamide containing 0.1 % pyridine. To enhance volatility and detection, 50 µL of N-methyl-N-(tert-butyldimethylsilyl)trifluoroacetamide (MBDSTFA, Macherey-Nagel)was added to both sample types for derivatization. The mixture was then incubated at 80 °C for 30 min to ensure complete derivatization. The derivatized samples were analyzed by GC-MS, and the resulting mass spectra were compared against the National Institute of Standards and Technology (NIST) library (version: NIST08) and mass spectra of related metabolites derivatized with MBDSTFA (Becker et al., 2005; Kiefer et al., 2004). Additionally, spectral comparisons were performed with derivatized pure compounds selected based on structural similarity and metabolic pathway architecture to confirm the identities of the detected intermediates.

2.11. Isotopic tracer studies and GC-MS ¹³C-labeling analysis

For the ^{13}C isotopic tracer experiments, cells were first cultivated in a preculture using BHI medium, followed by a second preculture in minimal medium supplemented with 55 mM 99 % [U- $^{13}\text{C}_6$]-glucose (Cambridge Isotope Laboratories) as the sole carbon source. The main culture was then grown in minimal medium containing 55 mM 99 % [U- $^{13}\text{C}_6$]-glucose and 5 mM naturally labeled *p*-coumarate, and inoculated at an initial OD₆₆₀ of 1.0 using the ^{13}C -labeled cells from the second preculture to eliminate interference from unlabeled biomass in the subsequent labeling analysis (Wittmann, 2007). Cells were harvested during exponential growth at OD₆₆₀ of 2.0, at which point both glucose and *p*-coumarate were still available. The cells were harvested during growth at OD₆₆₀ of 2.0.

For the 13 C analysis of proteinogenic amino acids, 1 mg of CDM was sampled (8.000×g, 4 min, 4 °C), washed twice with deionized water, hydrolyzed (6 M HCl, 24 h, 100 °C), and clarified from debris (Ultrafree-MC, 0.2 µm, Merck Millipore, Darmstadt, Germany). After drying under a nitrogen flow, the hydrolysate was dissolved in 50 µL of dimethylformamide (0.1 % pyridine) and derivatized with MBDSTFA (Macherey and Nagel) at 80 °C for 30 min (Wittmann and Heinzle, 2002), followed by GC–MS analysis (Hoffmann et al., 2018).

For the 13 C analysis of cellular sugars, 2.5 mg of CDM was sampled $(8.000\times g, 4 \text{ min}, 4 ^{\circ}\text{C})$ and washed twice with ultrapure water (Wittmann et al., 2004a). Hydrolysis was conducted in 250 μ L of 2 M HCl for 2 h at 100 $^{\circ}\text{C}$, followed by the removal of cell debris by filtration (Ultrafree-MC, 0.2 μ m, Merck Millipore, Darmstadt, Germany). After drying the hydrolysate under a nitrogen flow, the sample was processed in two steps, including an incubation in 100 μ L of methoxylamine (2 % pyridine) and subsequent derivatization using 100 μ L of *N,O*-bistri-methyl-silyl-trifluoroacetamide (BSTFA; Macherey and Nagel). For extracellular trehalose detection, 250 μ L of the supernatant generated at the time of sampling was also dried under nitrogen flow and processed as described for the cellular sugars. GC–MS was conducted as described previously (Kohlstedt and Wittmann, 2019).

For the 13 C analysis of fatty acids, 2.5 mg of CDM was sampled (8.000×g, 4 min, 4 °C), washed twice with deionized water, extracted and transesterified into the corresponding methyl esters (Dietrich et al., 2023). Briefly, the cells were dried for 60 min at 65 °C and 9 mbar in a vacuum concentrator (Savant DNA 120 SpeedVac, Thermo Fisher Scientific), dissolved in 300 μ L of a mixture of methanol, toluene, and 95 %

sulfuric acid (50:50:2; v/v/v), followed by an incubation at 80 °C for 15 h. After cooling to room temperature, the reaction was stopped by adding 250 µL of a stop solution (0.5 M NH₄HCO₃ and 2 M KCl in H₂O). After mixing for 30 s, the samples were centrifuged ($8000 \times g$, 5 min, RT), and the upper phase was used for GC-MS analysis (Gas chromatograph 7890B, Quadrupole Mass Selective Detector 5977A, Agilent Technologies) using an HP-5ms Ultra Inert column (30 m \times 250 μ m x 0.25 μ m, Agilent J&W) with helium 5.0 at 1.5 mL min⁻¹ as carrier gas. Inlet and auxiliary temperature were set to 280 °C. The oven temperature program was as follows: a ramp of 5 °C min⁻¹ from 130 °C to 175 °C, 175 °C for 5 min, 5 °C min⁻¹ from 175 °C to 210 °C, and 10 °C min⁻¹ from 210 °C to 320 °C, resulting in a total time of 33 min. The ¹³C labeling patterns of the methyl esters of palmitic acid (C16:0, m/z 270–286) and oleic acid (C18:1, m/z 296–314) were determined by analyzing their corresponding molecular ions. Non-labeled samples were analyzed in scan mode to confirm that the measured mass isotopomer distributions (MIDs) of the selected ion clusters matched theoretical isotope abundances. Subsequently, the ¹³C labeling patterns of the two cellular fatty acids were assessed in selective ion monitoring (SIM) mode.

All mass isotopomer distributions (MIDs) were corrected for the presence of naturally occurring isotopes (van Winden et al., 2002) and for the contribution of ¹³C-labeled metabolites originating from the inoculum. The resulting data represent mass isotopomer fractions corresponding solely to the carbon skeletons of the analytes. From these corrected values, the total ¹³C enrichment of each metabolite—referred to as summed fractional labeling (SFL)—was calculated as described previously (Schwechheimer et al., 2018a). SFL values are reported as percentages, with 100 % indicating complete ¹³C labeling of the carbon backbone.

2.12. Global gene expression analysis

For the analysis of global gene expression profiles in C. glutamicum strains under various conditions, customized one-color microarrays (SurePrint G3 Custom GE 8 \times 60K, part number G4102A, Agilent Technologies) were employed using previously established protocols (Christmann et al., 2023; Pauli et al., 2023). The array included probes for each gene in the C. glutamicum ATCC 13032 genome (Entry number #T00102, KEGG database), as well as for the heterologous genes aroY, ecdB, and ecdD from Enterobacter cloacae (Weiland et al., 2023). The genes were represented by three 45-60 bp probes, which were applied in six replicates and randomized across different slide locations using SurePrint technology (Agilent Technologies). For RNA extraction, C. glutamicum strains were cultivated under different conditions until they reached an OD660 of 4. At this point, 2 mL of culture broth was harvested by centrifugation (13,000×g, RT, 1 min), and the cell pellet was immediately frozen in liquid nitrogen. Simultaneously, culture supernatants were collected for an HPLC analysis of substrate conversion at the sampling time points. RNA was extracted and purified using the RNeasy Mini Kit (Qiagen, Hilden, Germany), followed by quantification using a NanoDrop 1000 spectrophotometer (PEQLAB Biotechnology, Erlangen, Germany) and quality control assessment with an RNA 6000 Nano Kit on an Agilent 2100 Bioanalyzer (Agilent Technologies). Only RNA samples with an RNA integrity number (RIN) > 9.0 were used for further analysis. For microarray hybridization, Cy3-labeled complementary RNA (cRNA) was generated using the Low Input Quick Amp WT Labeling One-Color Kit and RNA Spike-In One-Color Kit (Agilent Technologies). The labeled cRNA was then fragmented and hybridized to the microarrays using the Gene Expression Hybridization Kit (Agilent Technologies) according to previously described protocols (Christmann et al., 2023; Pauli et al., 2023). The data were analyzed using Gene-Spring (version 14.9; Agilent Technologies). Statistical significance was determined using an unpaired t-test (Benjamini-Hochberg correction, asymptotic p value computation), with a corrected p value cutoff of 0.05. Differentially expressed genes were identified by filtering the dataset for log_2 -fold changes greater than 2 or less than -2 (p value \leq

0.05). All RNA extraction and transcriptomic analyses were conducted in biological triplicates for each strain.

3. Results

3.1. Carbon catabolite repression limits efficient MA production from p-coumarate, ferulate, and caffeate in C. glutamicum

The metabolism of *p*-hydroxycinnamates in MA-producing *C. glutamicum* strains appears limited, restricting the efficient utilization of these valuable aromatic substrates from grassy plants for MA production (Weiland et al., 2023). We investigated this process by

culturing wild-type and *C. glutamicum* MA-6A on three *p*-hydroxycinnamates, *p*-coumarate, ferulate, and caffeate, and analyzed their metabolic dynamics. In all three setups, the *C. glutamicum* wild-type strain efficiently consumed glucose, which was supplemented as the primary growth substrate, during the exponential phase (Fig. 2A–C). The uptake of *p*-coumarate, ferulate, and caffeate was very weak when glucose was available, with the amount of assimilated carbon from these aromatics remaining below 2.9 % of the assimilated glucose carbon. However, once glucose was depleted after 10 h, the consumption of aromatics was strongly activated, leading to their rapid uptake.

A similar pattern was observed for the strain C. glutamicum MA-6A, where the delayed metabolism of aromatics imposed a significant

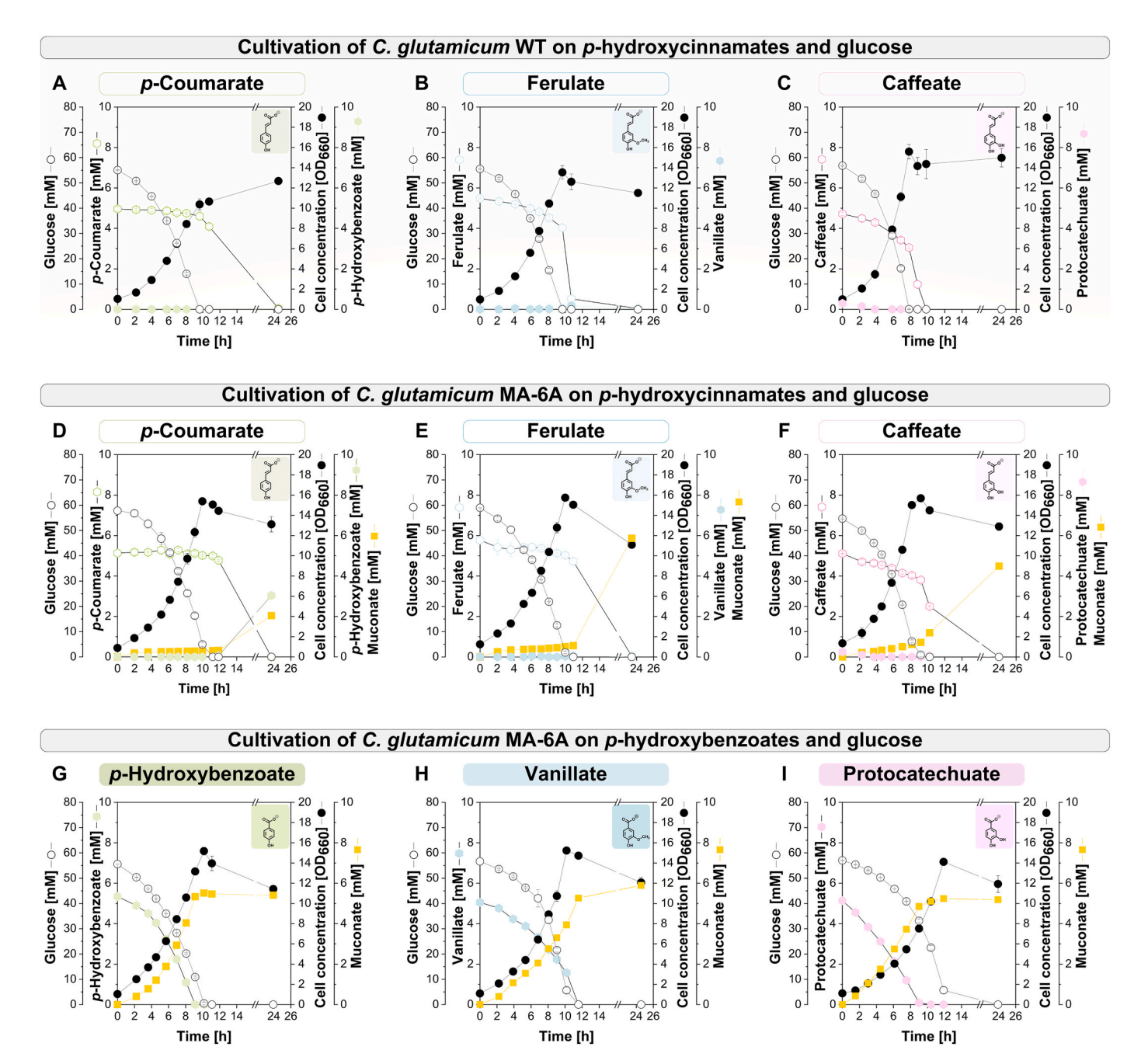


Fig. 2. Metabolic dynamics of *C. glutamicum* cultivated on mixtures of glucose and various *p*-hydroxycinnamates or *p*-hydroxybenzoates. Aromatic substrates—*p*-coumarate (A, D), ferulate (B, E), caffeate (C, F), *p*-hydroxybenzoate (G), vanillate (H), and protocatechuate (I)—were each supplied at a concentration of 5 mM in combination with 55 mM glucose. Panels A–C show the results for the wild-type strain, whereas panels D–I depict data from the engineered MA-producing strain MA-6A. The data for vanillate (Panel H) were obtained from previously published work (Weiland et al., 2023). The data are presented as the mean values and standard deviations from biological triplicates (n = 3).

limitation on MA production (Fig. 2D-F). The sequential uptake of substrates prolonged the overall process, as MA production remained negligible during the glucose-associated growth phase. Consequently, MA synthesis was confined to the later nongrowth stages of cultivation, where the absence of glucose likely led to energy and redox limitations, further constraining production efficiency. Interestingly, ferulate and caffeate were completely converted into MA, with no detectable accumulation of aromatic intermediates after 24 h. In contrast, p-coumarate appeared to be the least preferred among the three p-hydroxycinnamates. Previously, we observed the simultaneous uptake of glucose and aromatics, such as different aromatic aldehydes, by C. glutamicum (Weiland et al., 2023), and the microbe is generally known for its ability to utilize multiple carbon sources in parallel (Baritugo et al., 2018; Görke and Stülke, 2008). This finding made the observed carbon catabolite repression particularly surprising. Further tests revealed that the repression was specific to *p*-hydroxycinnamates. When strain MA-6A was cultured with the corresponding intermediates of p-coumarate, ferulate, and caffeate degradation, namely, p-hydroxvbenzoate, vanillate, and protocatechuate (Fig. 1), these compounds were readily co-consumed alongside glucose (Fig. 2G-I). These findings suggest that the observed repression is limited to the initial steps of p-hydroxycinnamate metabolism, whereas downstream intermediates remain unaffected. Cinnamate, the unsubstituted biosynthetic precursor of p-coumarate, ferulate, and caffeate in plants (Weiland et al., 2022), differs from the tested p-hydroxycinnamates in that it lacks any functional groups on its benzene ring. Matching previous reports for the wild type strain (Kallscheuer et al., 2016), strain MA-6A was unable to degrade cinnamate, independent of whether glucose was present, whereas its presumed downstream intermediate, benzoate, was readily cometabolized alongside glucose (Fig. S1, Supplementary File 1).

3.2. Fluorescent reporter analysis of glucose-mediated control of p-hydroxycinnamate utilization in C. glutamicum

Consequently, a deeper understanding of the metabolic network surrounding the phd operon appeared essential to increase MA production from various p-hydroxycinnamates. The operon consists of two divergently transcribed units flanking the central phdR gene: phdAT, which is positioned to the left and is involved in import and initial CoA activation, and phdBCDE, which is located to the right and facilitates side-chain removal from the benzene ring (Fig. 3A). The putative promoter regions were assigned to the 247 bp sequence upstream of phdA(cg0341) and the 190 bp sequence upstream of phdB (cg0344) (Fig. S2, Table S3, Supplementary File 1). The entire upstream regions of phdA and phdB were cloned upstream of the mCherry reporter gene into the episomal vector pClik 5a MCS to investigate the regulation of these promoters, generating two red-fluorescent reporter plasmids. These constructs enabled the expression of either P_{phdAT} mCherry or $P_{phdBCDE}$ mCherry, allowing separate monitoring of promoter activity. The two plasmids were introduced into the wild-type strain. The resulting reporter strains were cultivated in a microbioreactor system, allowing real-time monitoring of both the cell concentration and fluorescence, with the latter serving as an indicator of reporter gene expression. The growth medium was supplemented with glucose and a selection of aromatic compounds, including p-hydroxycinnamates (p-coumarate, ferulate, and caffeate), p-hydroxybenzoates (p-hydroxybenzoate, vanillate, and protocatechuate), cinnamate and benzoate, to simulate MA production conditions. Glucose-only medium served as a control to establish the baseline expression levels (Fig. 3B, C, 3D, 3E).

When cultured with *p*-coumarate and glucose, both *C. glutamicum* reporter strains exhibited a distinct biphasic response. During the glucose-supported growth phase, mCherry fluorescence remained low, indicating minimal expression of both *phd* transcriptional units. However, upon glucose depletion - marked by the abrupt termination of growth - the fluorescence signal increased sharply, suggesting derepression and activation of the operon (Fig. S3, Supplementary File 1). A

similar expression pattern—basal activation in the presence of glucose followed by strong induction upon glucose depletion—was observed for the other *p*-hydroxycinnamates, ferulate and caffeate (Fig. 3, Fig. S3, Supplementary File 1). Interestingly, although the expression levels were generally low during the initial phase, they remained significantly higher than those observed under glucose-only conditions. This finding suggested a basal level of *phd* cluster expression in the presence of glucose.

In contrast, cultures supplemented with p-hydroxybenzoate, vanillate, and protocatechuate, the terminal phd pathway intermediates (Fig. 1), exhibited drastically reduced fluorescence. This finding indicates that none of these compounds induced the phd operon, regardless of nutrient availability. Notably, cinnamate triggered phd operon activation, particularly in the absence of glucose (Fig. 3), despite the compound not being consumed (Fig. S4, Supplementary File 1). However, the resulting increase in fluorescence was significantly lower than that observed for p-hydroxycinnamates. Benzoate, like p-hydroxybenzoates, failed to induce the expression of the operon.

Interestingly, the $P_{phdBCDE}$ -based reporter plasmid consistently yielded greater fluorescence than did the plasmid containing P_{phdAT} (Fig. 3B and D), reflecting inherent differences in the native promoter strengths of the phd operon transcriptional units. This finding was further evidenced by the more intense coloration of the pelletized cells (Fig. 3C and E). Across all conditions and various degrees of induction, the $P_{phdBCDE}$ promoter, which regulates downstream enzymatic steps, displayed approximately three times greater activity than P_{phdAT} , which controls substrate import and CoA-thioester generation (Fig. 3F, Fig. S5, Supplementary File 1).

3.3. Intracellular p-coumaroyl-CoA-based intermediates reveal active phd-pathway flux in C. glutamicum MA-6A, despite glucose-repressing conditions

A metabolomic analysis of *C. glutamicum* MA-6A cultivated with glucose and *p*-coumarate revealed the presence of all key CoA-based intermediates involved in *p*-hydroxycinnamate metabolism, despite the repression of aromatic degradation by glucose (Fig. 4). Notably, the detection of intracellular *p*-coumaroyl-CoA, 3-hydroxy-*p*-coumaroyl-CoA, and 3-oxo-*p*-coumaroyl-CoA levels revealed that the entire pathway was active under these conditions. In previous studies, CoA-based metabolic intermediates were undetectable through indirect tracing of the corresponding acids (Kallscheuer et al., 2016), leaving its operation open. The latter two intermediates were 100-fold less abundant than *p*-coumaroyl-CoA was, based on signal intensities, and eventually escaped previous detection.

3.4. PhdR deletion specifically deregulates the phd operon, uncoupling it from the nutrient status

As shown, carbon catabolite repression impeded the efficient metabolism of p-coumarate, ferulate, and caffeate in the MA-producing strain C. glutamicum MA-6A in the presence of glucose (Fig. 3), negatively impacting MA production (Fig. 2). We aimed to delete the phdR gene, encoding the repressor of the phd operon, to overcome this limitation. PCR and sequencing confirmed the complete removal of phdR. The resulting mutant was designated C. glutamicum MA-10.

We conducted a microarray analysis to elucidate the transcriptional effects of the deletion in our MA-producing background. In the comparison of strains MA-6A and MA-10, glucose was used as the sole carbon source to eliminate potential secondary effects from an additional substrate. The cells were harvested in the midexponential phase, and principal component analysis confirmed the high statistical quality of the microarray data (Fig. S6, Supplementary File 1). The deletion of phdR significantly altered the expression of the seven pdh genes (Table 2, log_2 -fold change <-2 or >2, $p_{corr} \le 0.05$), indicating that PhdR was the major regulator in the presence of glucose and reinforcing its function as

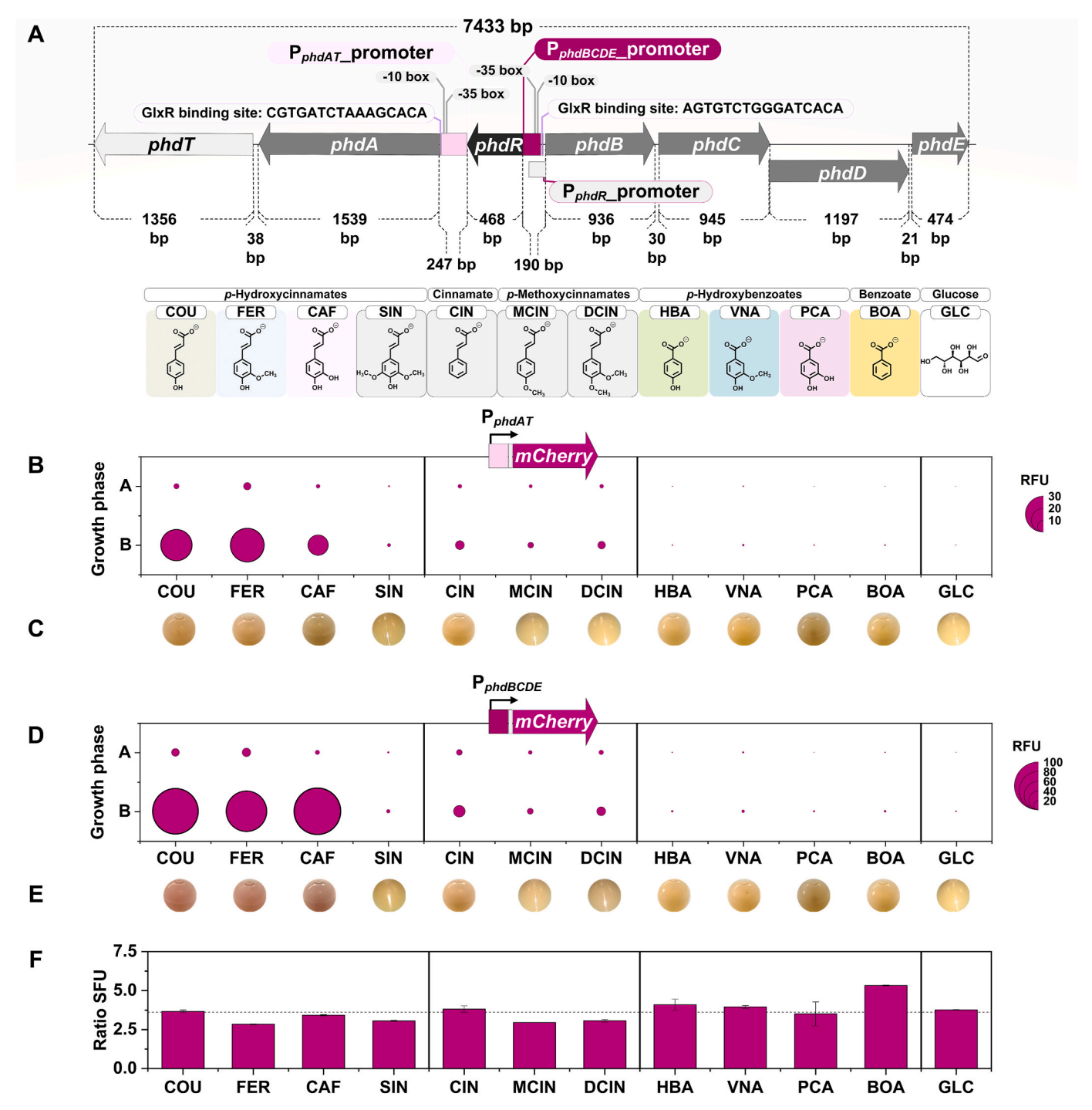


Fig. 3. Analysis of the expression of genes involved in *p*-hydroxycinnamate degradation using mCherry-based biosensors. Schematic representation of the *phd* operon (A). Promoter regions, –10 and –35 boxes, and GlxR-binding sites were identified using online prediction tools and previously published data (Kohl & Tauch, 2009) (Fig. S2, Table S3, Supplementary File 1). Reporter constructs were created by placing the mCherry gene under the control of the upstream regions of the transcriptional units *phdAT* and *phdBCDE* using the episomal vector pClik 5a MCS. These constructs were subsequently introduced into wild-type *C. glutamicum*. Sensor strains were cultivated in a microbioreactor, which monitored biomass and fluorescence during growth in media containing 55 mM glucose and 5 mM various aromatic compounds. The tested compounds included *p*-hydroxycinnamates and derivatives (COU—*p*-coumarate, FER—ferulate, CAF—caffeate, SIN-sinapinate, CIN—cinnamate, DCIN—3,4-dimethoxycinnamate, and MCIN—4-methoxycinnamate), as well as *p*-hydroxybenzoates and related compounds (HBA—*p*-hydroxybenzoate, VNA—vanillate, PCA—protocatechuate, and BOA—benzoate). Glucose-only medium (GLC) served as the control. The average mCherry fluorescence (relative fluorescence units, RFU; gain = 50) obtained for the *P*_{phdAT} (B) and *P*_{phdBCDE} (D) reporter strains was visualized in a bubble chart for two time points: at the end of the exponential growth phase ("A") and after 24 h ("B"). For each condition, 1 mL of cell broth was pelletized after cultivation for 24 h (P_{phdAT} (C) and P_{phdBCDE} (E)). The brownish color observed for experiments based on, e.g., caffeate, underly an additional darkening due to easy oxidation. The growth profiles can be found in Fig. S3, Supplementary File 1. Ratio of the average specific fluorescence units (Fig. S5) for the obtained signals representative for the promoter strengths of the P_{phdAT} and the P_{phdBCDE}-transcription units (F). The data are presented as the mean values and standard deviations

Metabolic Engineering 92 (2025) 262-283

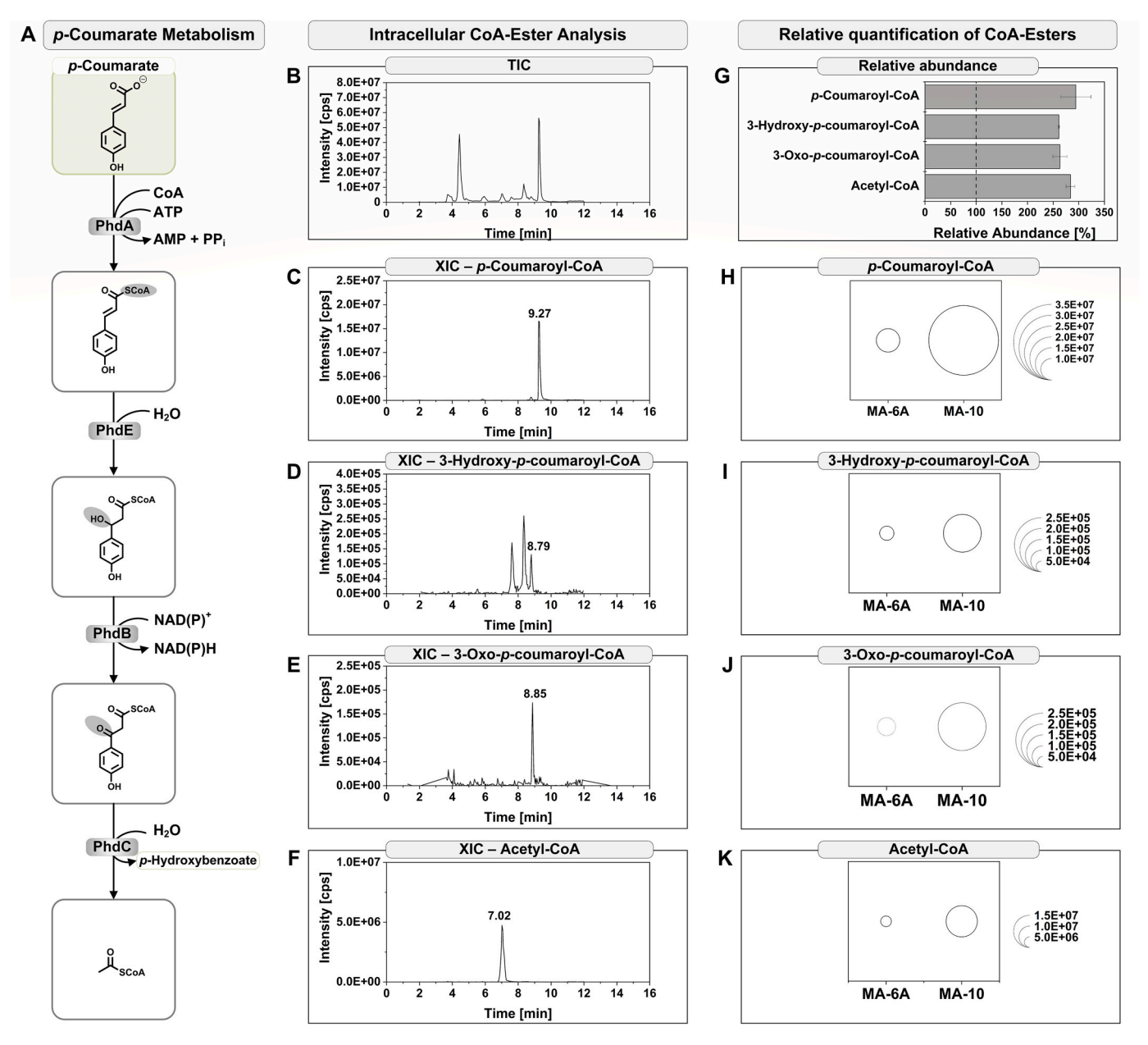


Fig. 4. Analysis of intracellular CoA esters involved in p-coumarate metabolism in strains MA-6A and MA-10. A schematic overview of CoA esters relevant for p-coumarate degradation in C. glutamicum is shown (A). Both strains were sampled at an OD₆₆₀ of 4 in minimal medium supplemented with 5 mM p-coumarate and 55 mM glucose. A representative total ion chromatogram (TIC) obtained for intracellular CoA-ester analysis of strain MA-10 via LC-MS/MS (B), as well as the respective extracted ion chromatograms (XIC) (C-F) for the pathway-relevant metabolites p-coumaroyl-CoA, 3-hydroxy-p-coumaryl-CoA, 3-oxo-p-coumaroyl-CoA and acetyl-CoA, are shown. For relative quantification, the analyte peak area (counts) obtained via LC-MS/MS analysis was normalized to an OD₆₆₀ value of 1. Comparison of the relative abundance of different intracellular CoA esters in C. glutamicum MA-10 with that of strain MA-6A with respect to native p-hydroxycinnamate metabolism (set to 100 %, indicated by a dashed line) (G). Bubble chart of each CoA-ester (H–K), where the circle size reflects the relative abundance of each metabolite. The data are presented as the mean values and standard deviations from biological duplicates (n = 2).

a specific repressor of p-hydroxycinnamate metabolism (Kallscheuer et al., 2016). Notably, the change in phdAT expression (log₂-fold change of 4.7–5.4) was significantly less pronounced than that of the phdBCDE operon (log₂-fold change of 6.7–7.9). This observation aligned well with the observed differences in promoter strength between the two transcriptional units, as discovered using the biosensor strains (Fig. 3).

3.5. GlxR integrates p-hydroxycinnamate catabolism into the carbon catabolite repression network

Notably, multiple binding sites of the global regulator GlxR (Schröder & Tauch, 2010) were identified upstream of the phd operon

(Kohl & Tauch, 2009), although the function of this operon was not known at the time (Fig. 3A, Fig. S2, Supplementary File 1). From a production perspective, deletion of *phdR* was sufficient to derepress the operon (Table 2), suggesting that GlxR was not a limiting factor for *phd* pathway flux. However, given the central role of GlxR in carbon catabolite repression of *C. glutamicum* and the presence of multiple binding motifs, it appeared both interesting and relevant to further investigate its specific regulatory influence on the *phd* operon, particularly in the context of glucose availability.

To test the functionality of the GlxR binding sites and assess their regulatory role, we constructed two sensor plasmids in which the GlxR binding motifs were removed from the promoter regions. Similar

Table 2 Transcriptional analysis of the impact of *phdR* deletion on gene expression in *C. glutamicum* MA-10 cultivated in glucose compared with its parental strain MA-6A. Both strains were cultivated in minimal medium supplemented with glucose as the sole carbon source and harvested at an OD₆₆₀ of 4. Differential gene expression was assessed using an unpaired *t*-test, and the Benjamini–Hochberg correction was applied for multiple testing. A gene was considered significantly differentially expressed if it met the following criteria: p_{corr} value ≤ 0.05 and $|log_2(fold change)| > 2$ or < -2. Protein annotations were obtained from the NCBI database (https://www.ncbi.nlm.nih.gov/).

NCgl number	CGL number	Cgl number	Gene name	NCBI annotation	Log2(FC)	p _{Corr} -value
NCgl0278	CGL_RS01485	Cgl0283	phdT	MFS transporter	5.38	2.56E-07
NCgl0279	CGL_RS01490	Cg10284	phdA	Long-chain fatty acid-CoA ligase	4.67	1.65E-07
NCgl0280	CGL_RS01495	Cg10285	phdR	MarR family winged helix-turn-helix transcriptional regulator	-7.62	2.57E-09
NCgl0281	CGL_RS01500	Cg10286	phdB	SDR family NAD(P)-dependent oxidoreductase	6.79	2.57E-09
NCg10282	CGL_RS01505	Cg10287	phdC	4-Hydroxyphenyl-beta-ketoacyl-CoA hydrolase	6.68	4.35E-08
NCgl0283	CGL_RS01510	Cg10288	phdD	Acyl-CoA dehydrogenase family protein	7.88	2.57E-09
NCgl0284	CGL_RS01515	Cg10289	phdE	MaoC family dehydratase	6.75	1.43E-07

strategies have been employed previously to dissect transcriptional regulation in C. glutamicum, including the mutation and deletion of GlxR binding motifs to study the regulation of different catabolic genes (Morabbi Heravi et al., 2015; Toyoda et al., 2009a, 2009b). One of the plasmids was designed to monitor mCherry expression under control of the P_{phdAT} promoter lacking GlxR binding (P_{phdAT}^{mut}), and the other under control of the $P_{phdBCDE}$ promoter, also lacking GlxR binding ($P_{phdBCDE}^{mut}$). These plasmids were introduced into C. glutamicum wild type for further analysis. The resulting sensor strains were cultivated on media containing *p*-coumarate and glucose, ferulate and glucose, or glucose alone. Growth and mCherry fluorescence were monitored in real time. While P_{phdBCDE} mCherry showed a strong increase in fluorescence, following glucose depletion (Fig. 5), the mutated promoter $P_{phdBCDE}^{mut}$ yielded only a modest induction, indicating that GlxR plays a critical role in activating the *phdBCDE* operon under glucose-limited conditions in *C. glutamicum*. In contrast, fluorescence dynamics for P_{phdAT} and P_{phdAT}^{mut} were largely similar, with the native promoter showing a slightly higher expression (10 % on average) after glucose depletion than the mutated version. These results suggest that GlxR exerts a modest but significant activating effect on the phdAT operon. Similar characteristics were observed at lower glucose concentrations, indicating that the observed effects reflect a general pattern of carbon catabolite regulation (Fig. 5, 7 and 8, Supplementary File 1).

Together, these findings demonstrated that GlxR serves as a key activator of the *phdBCDE* operon under glucose-limited conditions, while exerting a more moderate but detectable influence on *phdAT* expression. This regulatory pattern highlights the role of GlxR in coordinating the expression of aromatic degradation genes with carbon availability. As such, the *phd* operon appears to be integrated into the broader carbon catabolite repression network of *C. glutamicum*, ensuring prioritized glucose utilization while enabling efficient aromatic compound catabolism upon glucose depletion. Notably, GlxR was also shown to contribute to 3-hydroxybenzoate and gentisate metabolism in *C. glutamicum* (Chao and Zhou, 2014).

3.6. C. glutamicum MA-10 produces MA at increased rates, titers, and yields

Next, MA-10 was evaluated for MA production from p-coumarate (Fig. 6A) and ferulate (Fig. 6E), the two major lignocellulose-derived p-hydroxycinnamates, to assess the impact of phdR deletion on performance. Notably, both p-coumarate and ferulate were rapidly consumed from the start of cultivation and were stoichiometrically converted into MA within just 12 h. Strain MA-10 co-consumed 4.89 mM p-coumarate alongside glucose during the initial culture phase (7.1 h), which was 99.7-fold higher than that of MA-6 (0.05 mM) (Fig. 2). Ferulate was metabolized more efficiently than p-coumarate, which is consistent with strain MA-6A (Fig. 2). Compared with that of MA-6A, its co-consumption increased 15-fold (5.42 mM vs. 0.36 mM during the first 5.1 h). The decoupled metabolism of both substrates led to the transient accumulation of terminal phd pathway intermediates, with a more pronounced

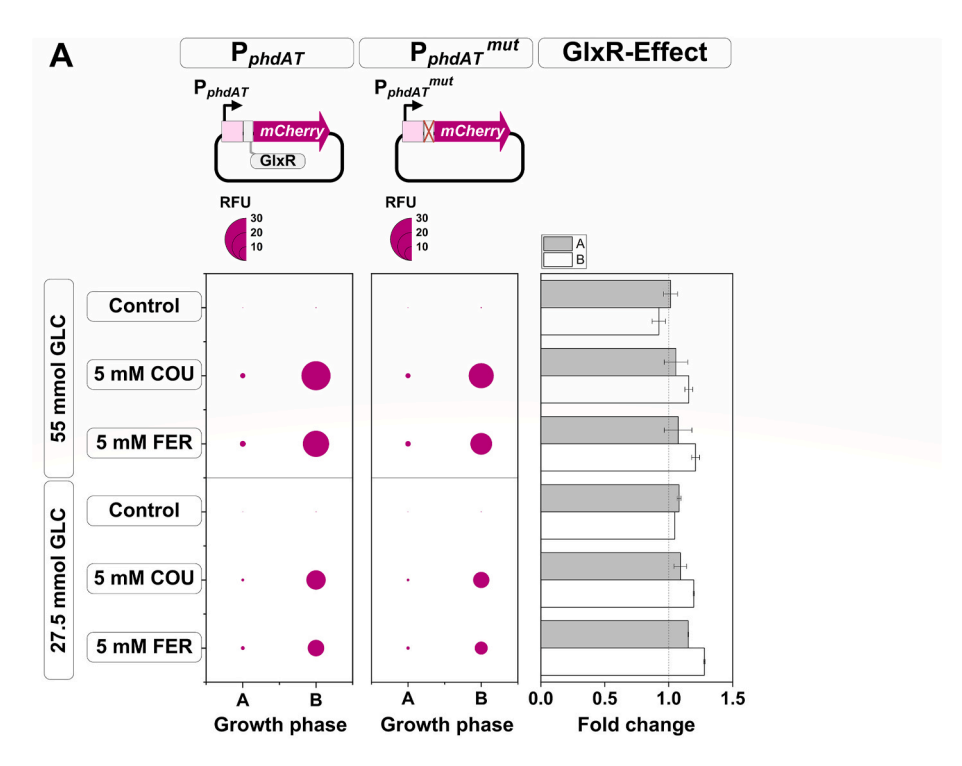
and rapid effect on the ferulate-based process. Specifically, p-hydroxybenzoate accumulated up to 3.4 \pm 0.1 mM after 6 h of cultivation with p-coumarate, whereas vanillate reached 4.2 \pm 0.1 mM after just 4 h of cultivation with ferulate. Afterward, both intermediates were efficiently co-consumed alongside their respective aromatic substrates, contributing to optimized metabolic flux toward MA.

The correlation of substrate dynamics over time—specifically, the relative consumption of glucose, aromatic substrates, and their intermediates—revealed a dramatically altered utilization pattern in strain MA-10 (Fig. 6B and F). Unlike MA-6A, where aromatic metabolism was nearly negligible in the presence of glucose due to repression, MA-10 exhibited efficient cometabolization throughout the entire process. This co-consumption occurred regardless of whether p-coumarate or ferulate or their intermediates were present, indicating that phd pathway deregulation enabled the robust and simultaneous processing of both glucose and aromatics, in stark contrast to the restricted utilization observed in MA-6A under glucose-repressive conditions (Fig. 2). Taken together, phdR deletion enabled the complete conversion of the supplied aromatics into MA by the time glucose was depleted and growth ceased, leading to 48-fold and 18-fold increases in MA yields at this time point (Fig. 6C and G) for p-coumarate and ferulate, respectively. Moreover, the MA yield, relative to the supplied amount of glucose, was significantly improved (Fig. 6D and H).

3.7. The deletion of phdR increases the efficiency of substrate utilization towards higher concentration levels

In the context of lignin upgrading, microbial cell factories should be featured by a high tolerance to elevated concentrations of the toxic aromatic substrates (Becker and Wittmann, 2019), making efficient conversion at elevated substrate concentrations a key advantage. To this end, C. glutamicum MA-6A and MA-10 were benchmarked by cultivating both strains with increased p-coumarate and ferulate levels (up to 30 mM) alongside glucose (Fig. 7), with the growth curves provided in Fig. S9 (Supplementary File 1). In MA-6A, lower p-coumarate concentrations (<10 mM) caused p-hydroxybenzoate accumulation, whereas at concentrations above 15 mM, the majority of the supplied p-coumarate remained unconverted. In contrast, MA-10 exhibited significantly improved performance across all tested conditions. The mutant fully converted 15 mM p-coumarate into MA within 24 h, and even at the highest concentrations tested, biotransformation was evident, as indicated by the accumulation of p-hydroxybenzoate and muconate in the supernatant. Similarly, ferulate conversion was markedly increased in MA-10, enabling complete utilization of 15 mM ferulate within 24 h. These results highlight the substantial benefits of phdR deletion in increasing overall strain efficiency.

Additionally, caffeate consumption was highly improved in strain MA-10 across varying concentration levels indicating continuous enhancing effects of phdR-deletion on the metabolism of p-hydroxycinnamates naturally belonging to the substrate spectrum of C. C0, C1, C2, C3, C4, C5, C5,



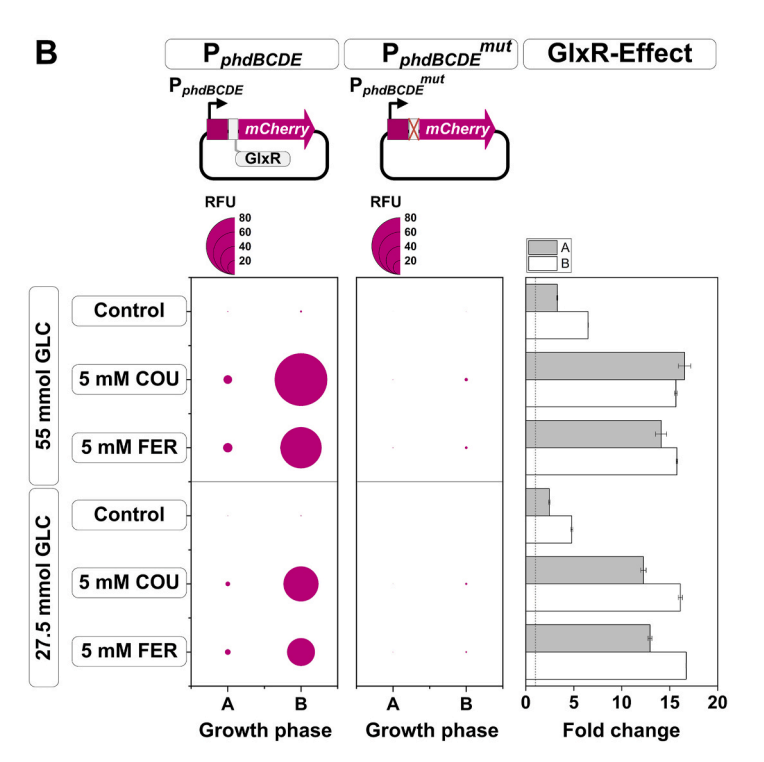


Fig. 5. Functional analysis of GlxR-mediated regulation of the *phd* operon using mCherry-based biosensors. To assess the regulatory role of GlxR, reporter constructs were created in which the GlxR-binding motifs were removed from the *phdAT* (A) and *phdBCDE* (B) promoter regions, generating the P_{phdAT}^{mut} and $P_{phdBCDE}^{mut}$ constructs, respectively. The mCherry gene was placed under control of the mutated promoters using the episomal vector pClik 5a MCS, and the resulting plasmids were introduced into wild-type *C. glutamicum*. Sensor strains were cultivated in media containing 55 mM or 27.5 mM glucose with either 5 mM *p*-coumarate or 5 mM ferulate, or glucose alone. Fluorescence intensities (relative fluorescence units, RFU; gain = 50) of the reporter strains P_{phdAT} and P_{phdAT}^{mut} (A) and for $P_{phdBCDE}$ and $P_{phdBCDE}^{mut}$ (B) were visualized in a bubble chart for two time points: at the end of the exponential growth phase ("A") and after 24 h ("B"). In addition, the ratios of the average relative fluorescence units between native and mutated promoters are given, visualizing the transcriptional effects of GlxR at both time points. The data are presented as the mean values and standard deviations from biological triplicates (n = 3).

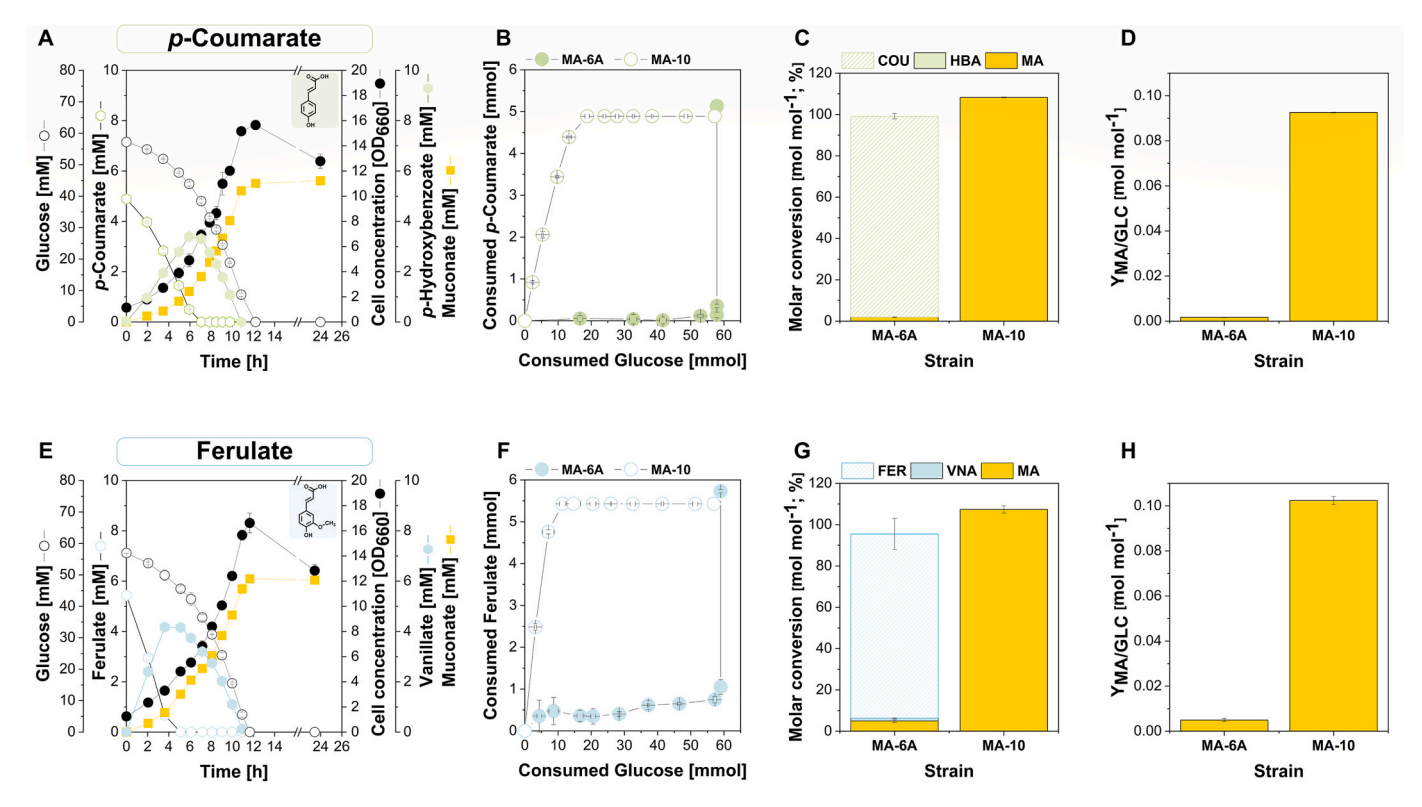


Fig. 6. p-Hydroxycinnamate-based MA production using the metabolically engineered C. glutamicum MA-10. Strain MA-10 was cultivated using the same method as its parent strain with native phd expression in the presence of 55 mM glucose and 5 mM p-coumarate (top panel) or 5 mM ferulate (bottom panel) in shake flasks. The shake flask profiles (A, E) and the resulting substrate uptake plots (B, F) are shown. The product yields shown here refer either to the supplied concentrations of the respective aromatics (C, C) or to the glucose concentration in the medium (C), C1. Product yields were calculated for the first sampling point of glucose depletion, whereby C2 is, C3 is muconate concentrations were corrected for the supplied small concentration of protocatechuate available in the medium as a chelating agent. The data are presented as the mean values and standard deviations from biological triplicates (C1) is C2.

observation during enhanced hydroxycinnamate conversion was the transient accumulation of downstream aromatic intermediates, specifically *p*-hydroxybenzoate and vanillate (Fig. 6), which became more pronounced at higher aromatics levels (Fig. S11, Supplementary File 1). A comparable bottleneck has been reported in *P. putida* KT2440, where accumulation of these intermediates was mitigated by overexpressing *vanAB* and replacing *pobA* with more efficient monooxygenases (Johnson et al., 2017; Kuatsjah et al., 2022; Salvachua et al., 2018; Werner et al.) Consistent with these findings and recent work in *C. glutamicum* (Weiland et al., 2023), our results indicate that byproduct-free muconate production might require increased flux through these monooxygenase steps to prevent intermediate buildup. Monooxygenase activity thus represents an interesting metabolic engineering target in the efficient catabolism of hydroxycinnamates in *C. glutamicum*.

3.8. C. glutamicum MA-10 exhibits increased availability of aromatic CoA thioesters and acetyl-CoA

Interestingly, the metabolomic analysis of *C. glutamicum* MA-10 cultivated with glucose and *p*-coumarate revealed significant differences in the availability of *phd* pathway-specific intracellular CoA esters compared with MA-6A. In contrast, strain MA-10 presented an approximately threefold increase in the abundance of all aromatic CoA esters (Fig. 4), indicating a substantial increase in *p*-hydroxycinnamate pathway flux following *phdR* deletion. Notably, while the overall pool sizes increased, the relative ratios between the individual CoA intermediates remained unchanged compared with those of MA-6A, with *p*-coumaroyl-CoA consistently dominating the CoA pool.

Additionally, MA-10 exhibited a three-fold increase in acetyl-CoA levels, stoichiometrically aligning with the elevated abundance of

aromatic CoA esters (Fig. 4). This suggested that p-hydroxycinnamate metabolism significantly impacts central carbon metabolism, even though the two processes initially appeared disconnected due to disrupted aromatic catabolism (Fig. 1). Notably, the intracellular level of succinyl-CoA—an intermediate of the TCA cycle—was 20 % lower in MA-10 compared to MA-6A (normalized peak area: 3.19×10^7 vs. 4.04×10^7), suggesting even broader perturbations of central metabolism by the engineered co-utilization of p-coumarate and glucose.

3.9. Isotopic analysis demonstrates a significant contribution of phenylpropanoid side chain–derived acetyl-CoA carbon to central metabolic pathways in strain MA-10

To investigate potential metabolic cross-talk between p-hydroxycinnamate degradation and central carbon routes in strain MA-10, we designed a¹³C-labelling experiment that allowed investigating the parallel metabolization of glucose and p-coumarate through analysis of ¹³C labelling patterns in cellular metabolites, a strategy proven valuable for resolving the metabolism complex substrate mixtures (Adler et al., 2013; Schulze et al., 2022; Schwechheimer et al., 2018b). To this end, strain MA-10 was grown on $[U^{-13}C_6]$ glucose and naturally labeled p-coumarate, followed by mass spectrometric analysis of representative major biomass constituents, including amino acids (proteins), ribose (nucleotides), fatty acids (lipids), and different hexoses (cell wall), as well as secreted products (trehalose, MA). These metabolites collectively span key nodes in the central carbon metabolism of C. C0.

The labeling patterns revealed substantial incorporation of ¹²C into multiple metabolites, indicating efficient assimilation of carbon from *p*-coumarate degradation into central metabolic pathways (Fig. 8A). Notably, ¹²C-enrichment was especially pronounced in metabolites directly derived from acetyl-CoA, such as fatty acids, which exhibited a

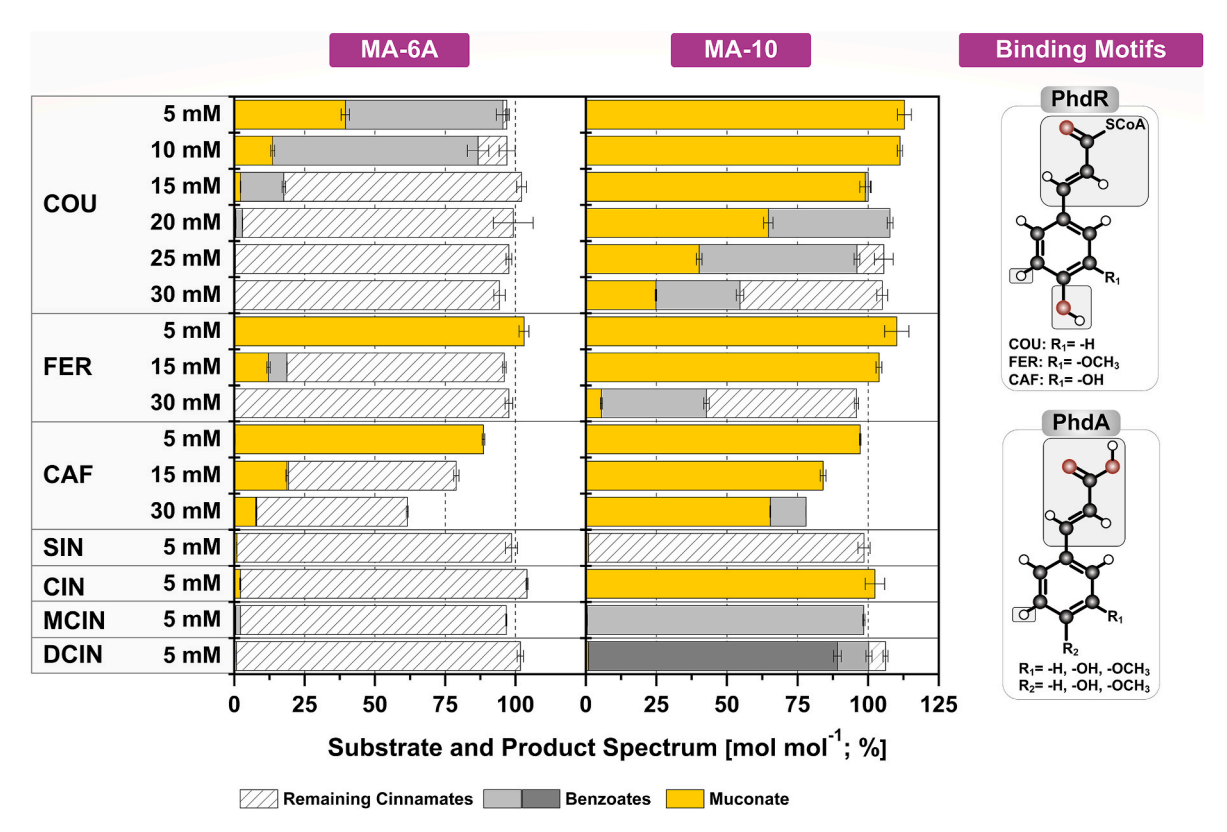


Fig. 7. Comparison of cinnamate conversion in strains MA-6A and MA-10. The strains were cultivated on various *p*-hydroxycinnamates (COU: *p*-coumarate, FER: ferulate, CAF: caffeate), cinnamate (CIN), and *p*-methoxycinnamates (MCIN: 4-methoxycinnamate, DCIN: 3,4-dimethoxycinnamate) at concentrations ranging from 5 to 30 mM, together with 55 mM glucose. Strain performance was compared by end point measurements taken after 24 h. *Cis.*, *cis.*-muconate concentrations were corrected for the supplied small concentration of protocatechuate available in the medium as a chelating agent. For 3,4-dimethoxycinnamate, two different benzoates were detected in the supernatant, where veratrate is depicted in light gray and the isovanillate is depicted in dark gray. The data are presented as the mean values and standard deviations from biological triplicates (n = 3). While PhdA acts on *p*-hydroxycinnamates and cinnamates, PhdR binds the corresponding CoA esters as effectors, similar to other bacteria (Otani et al., 2016; Kasai et al., 2012).

¹²C-fraction of approximately 70 %. This enrichment pattern strongly suggests that p-coumarate catabolism contributes significantly to acetyl-CoA pools via cleavage of the p-hydroxycinnamate side chain, facilitating its downstream integration into core biosynthetic routes. The active routing of acetyl-CoA into the TCA cycle was evidenced by significant 12C-enrichment in 2-oxoglutarate-derived amino acids, including glutamate, proline, and arginine. Furthermore, substantial ¹²C fractions were detected in amino acids derived from oxaloacetate, providing compelling evidence for the operation of the glyoxylate shunt. This is consistent with the bypass of oxidative decarboxylation at 2-oxoglutarate in the glyoxylate cycle, which prevents loss of the ¹²C carbons from p-coumarate based acetyl-CoA into CO2 and preserves its carbon skeleton for biosynthesis. Surprisingly, ¹²C-enriched carbon was detected even in nucleotide and cell wall sugars, derived from fructose 6phosphate, glucose 6-phosphate, and ribose 5-phosphate, suggesting active gluconeogenesis and a global distribution of carbon from the side chain of the aromatic within central metabolism. This points to a distinct metabolic advantage conferred by strain MA-10, wherein acetyl-CoA serves as an additional precursor for biomass formation. These results suggest a functional integration—or "division of labor"—between aromatic compound degradation and central metabolism. MA was naturally labeled, suggesting that it was formed from p-coumarate without significant contribution of the alternative route from glucose via pathway intermediates of aromatic amino acid synthesis.

3.10. Sugar-free MA production from p-hydroxycinnamates

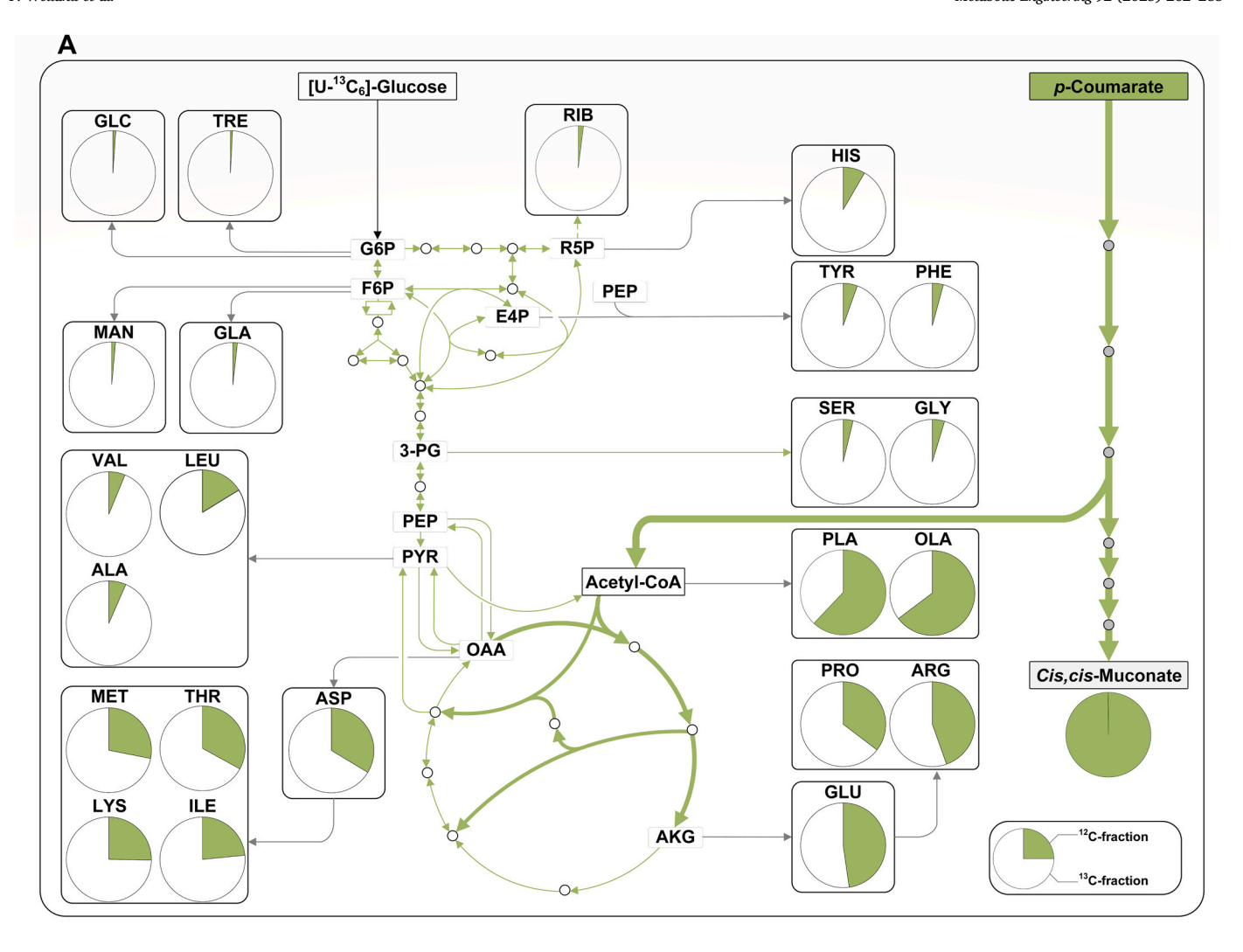
The evident metabolic crosstalk between p-hydroxycinnamate degradation and biomass formation via acetyl-CoA (Fig. 8A) inspired a

shift in strategy to completely abandon sugar and rely solely on an aromatic compound to fuel both growth and production. We challenged strain MA-10 with an increased level of 30 mM p-coumarate as the sole carbon and energy source. Astonishingly, within 24 h, 2.2 mM MA accumulated—clear proof of concept that sugar-free production is feasible (Fig. 8B, Fig. S12, Supplementary File 1). Even more striking was the 50 % increase in cell concentration, underscoring that acetyl-CoA derived from the aromatic side chain was sufficient to sustain energy generation, redox balancing, and biosynthesis. All non-MA carbon from *p*-coumarate was routed to the intermediate *p*-hydroxybenzoate. Intriguingly, the conversion rate from p-coumarate to p-hydroxybenzoate in the sugar-free setup outpaced that observed in glucosesupplemented cultures, which, despite reaching higher cell densities, left a substantial portion of p-coumarate unused (Fig. 8C). This highlights not only the metabolic efficiency of aromatic-driven growth but also reveals a potential regulatory tradeoff when sugars are present.

3.11. MA production from aromatic mixtures and straw lignin hydrolysates

Real-world lignin hydrolysates contain complex mixtures of aromatics, and advancing their microbial valorization requires a deeper understanding of aromatic co-metabolism (Becker et al., 2018a; Kohlstedt et al., 2018; Salvachua et al., 2018). Therefore, the strains MA-6A and MA-10 were cultivated on an equimolar mixture containing *p*-coumarate, ferulate, and their corresponding pathway intermediates, *p*-hydroxybenzoate and vanillate (Fig. 1).

Overall, the deregulated *phd* pathway in MA-10 enabled the efficient cometabolism of mixed aromatic compounds, further supporting its



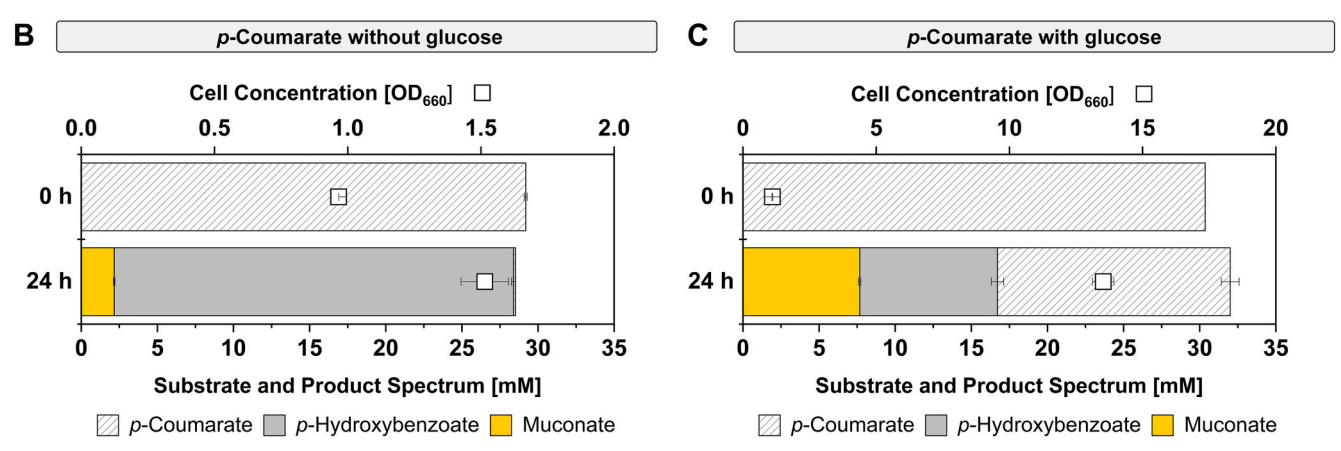


Fig. 8. Metabolic cross talk between p-coumarate degradation and central carbon metabolism in C. glutamicum MA-10. 13 C Metabolic flux analysis during cometabolism of glucose and p-coumarate (A). To elucidate substrate-specific carbon fluxes, C. glutamicum MA-10 was cultivated in minimal medium supplemented with $[U^{-13}C_6]$ glucose (55 mM) and unlabeled p-coumarate (5 mM). Cells were harvested at mid-exponential phase (OD $_{660} = 2$), ensuring the concurrent availability of both carbon sources. Isotopic labeling patterns were quantified by GC/MS in biomass-derived metabolites, including proteinogenic amino acids, peptidoglycan-and arabinogalactan-associated sugars, and lipid-derived fatty acids, as well as secreted metabolites such as cis, cis-muconate and trehalose. Mass isotopomer distributions were corrected for natural isotope abundance and inoculum, and ^{13}C enrichment levels were computed to infer the relative carbon contributions from glucose and p-coumarate to central and peripheral metabolic pools. MA production from glucose and p-coumarate (B) and from p-coumarate alone (C).

potential for lignin valorization applications (Fig. 9). In MA-6A, inhibitory effects of carbon catabolite repression on MA production were evident. The strain initially metabolized only *p*-hydroxybenzoate and vanillate, while *p*-hydroxycinnamate metabolism remained suppressed (Fig. 9A). As a result, MA titers plateaued once the two *p*-hydroxybenzoates were fully consumed. Only after glucose depletion did *p*-coumarate and ferulate consumption begin, leading to a delayed restart of MA production. In contrast, MA-10 enabled the efficient cometabolism of mixed aromatic compounds (Fig. 9B). The strain exhibited the simultaneous consumption of *p*-coumarate and ferulate, overcoming repression and accelerating aromatic metabolism with only a transient accumulation of benzoates during the initial process phase. This shift resulted in a substantial increase in MA levels, with higher yields achieved before glucose depletion, indicating improved production efficiency.

Next, *C. glutamicum* MA-10 was evaluated for MA production using Biolignin as a lignin source. Base-catalyzed hydrolysis of the strawderived lignin yielded a dark brown solution containing p-coumarate (1.04 mM) and ferulate (0.78 mM) as the predominant aromatic constituents (Fig. 8C). GC-MS analysis additionally revealed the presence of three minor aromatic compounds - p-hydroxybenzoate, vanillate, and vanillin (Fig. S13, Supplementary File 1) - whose concentrations in the hydrolysate, determined by HPLC, were 0.03 mM, 0.11 mM, and 0.14 mM, respectively (Fig. 9C, Fig. S14, Supplementary File 1).

The hydrolysate was added as the sole aromatic carbon source to

MA-10 cultures at 20 %, 40 %, and 60 % (v/v) concentrations in minimal medium supplemented with glucose. After 24 h, the culture containing 20 % hydrolysate produced 0.42 \pm 0.01 mM MA. Increasing the hydrolysate concentration to 40 % and 60 % (v/v) led to MA titers of 0.89 \pm 0.01 mM and 1.35 \pm 0.03 mM, respectively—representing approximately two- and three-fold increases. On average, 86.9 % of the MA carbon formed after 24 h could be attributed to the five aromatics. This indicates that p-hydroxycinnamates and their downstream intermediates served as the principal substrates for MA biosynthesis. Within error, the remaining MA fraction likely arises from additional aromatic compounds present at low concentrations, which were upgraded by C. glutamicum MA-10. Their identification will be the focus of future studies.

3.12. Expanded substrate range in C. glutamicum MA-10: metabolism of p-methoxylated cinnamates

The metabolism of the previously unexplored methoxylated cinnamate derivatives 4-methoxycinnamate, 3,4-dimethoxycinnamate, and 3,5-dimethoxy-4-hydroxycinnamate (sinapinate) was evaluated in *C. glutamicum*. Similar to cinnamate, these aromatic compounds also induced the *phd* operon, particularly in the absence of glucose (Fig. 3). However, the fluorescence levels were rather low and remained stable throughout cultivation, in contrast to the strong induction observed for the *p*-hydroxycinnamates ferulate and *p*-coumarate (Fig. S3,

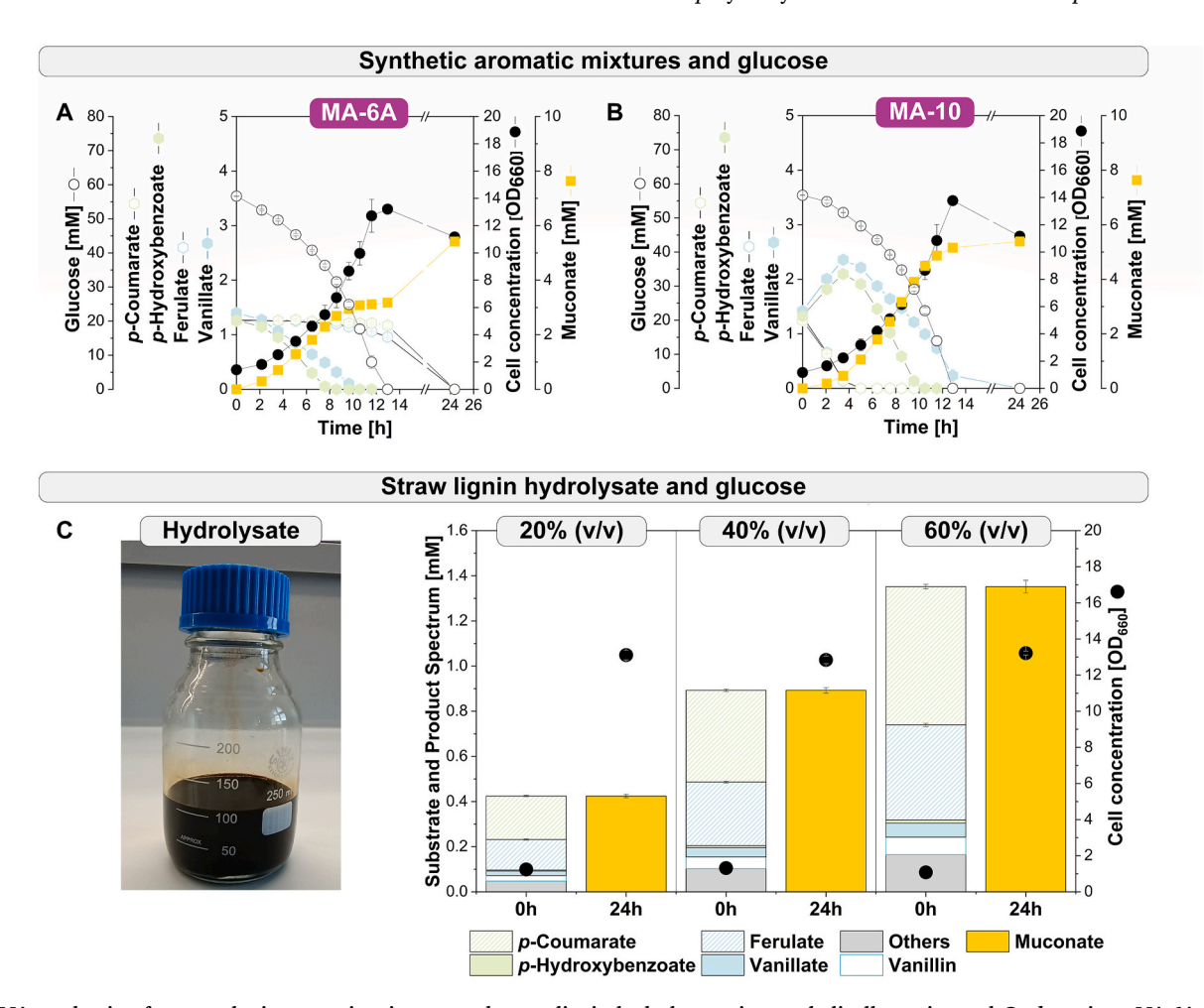


Fig. 9. MA production from synthetic aromatic mixtures and straw lignin hydrolysates in metabolically engineered C. glutamicum MA-6A and MA-10. C. glutamicum MA-6A (A) and MA-10 (B) were cultivated in the presence of 1.25 mM ferulate, p-coumarate, vanillate, p-hydroxybenzoate plus 55 mM glucose in shake flasks. Strain MA-10 was additionally cultivated in shake flasks in the presence of 20 % (ν/ν), 40 % (ν/ν) and 60 % (ν/ν) lignin hydrolysate, obtained from base-catalyzed depolymerization of straw lignin (Biolignin, CIMV) plus 55 mM glucose (C). The data reflect the concentrations of MA, other aromatic compounds, and the cell concentration (OD₆₆₀) at the beginning and after 24 h. The data are presented as the mean values and standard deviations from biological triplicates (n = 3).

Supplementary File 1).

Interestingly, unlike the wild-type strain (Fig. S4, Supplementary File 1) and the MA-6A strain, *C. glutamicum* MA-10 presented a highly expanded substrate spectrum (Fig. 7). Thus, *phdR* deletion facilitated cinnamate degradation, leading to MA formation *via* the native benzoate degradation pathway. Additionally, *C. glutamicum* MA-10 also metabolized the 4-methoxylated cinnamates, i.e., 4-methoxycinnamate and 3,4-dimethoxycinnamate, into novel compounds, as detected by HPLC analysis (Fig. 7, Fig. S15, Supplementary File 1). The supernatants were dried, derivatized and analyzed via GC–MS to characterize these unknown products. Guided by the metabolic layout of *p*-hydroxycinnamate degradation (Fig. 1) and validated by the analysis of pure standards, the

novel dead-end metabolites were identified as anisate (4-methoxybenzoate) resulting from 4-methoxycinnamate metabolization and veratrate (3,4-dimethoxy-benzoate) resulting from 3,4-dimethoxycinnamate (Fig. S16 and 17, Supplementary File 1). According to the results of the GC–MS and HPLC analyses, veratrate seemingly underwent further *O*-demethylation into isovanillate (Fig. 7).

Considering metabolic flexibility in aromatic degradation (Weiland et al., 2022), the vanillate-O-demethylase VanAB was deleted in strain MA-10 to investigate its potential contribution to 3,4-dimethoxycinnamate metabolism. Cultivation of the *vanAB*-deficient MA-11 mutant on 3,4-dimethoycinnamate and glucose resulted in the accumulation of veratrate without isovanillate formation (Fig. S18 and 19,

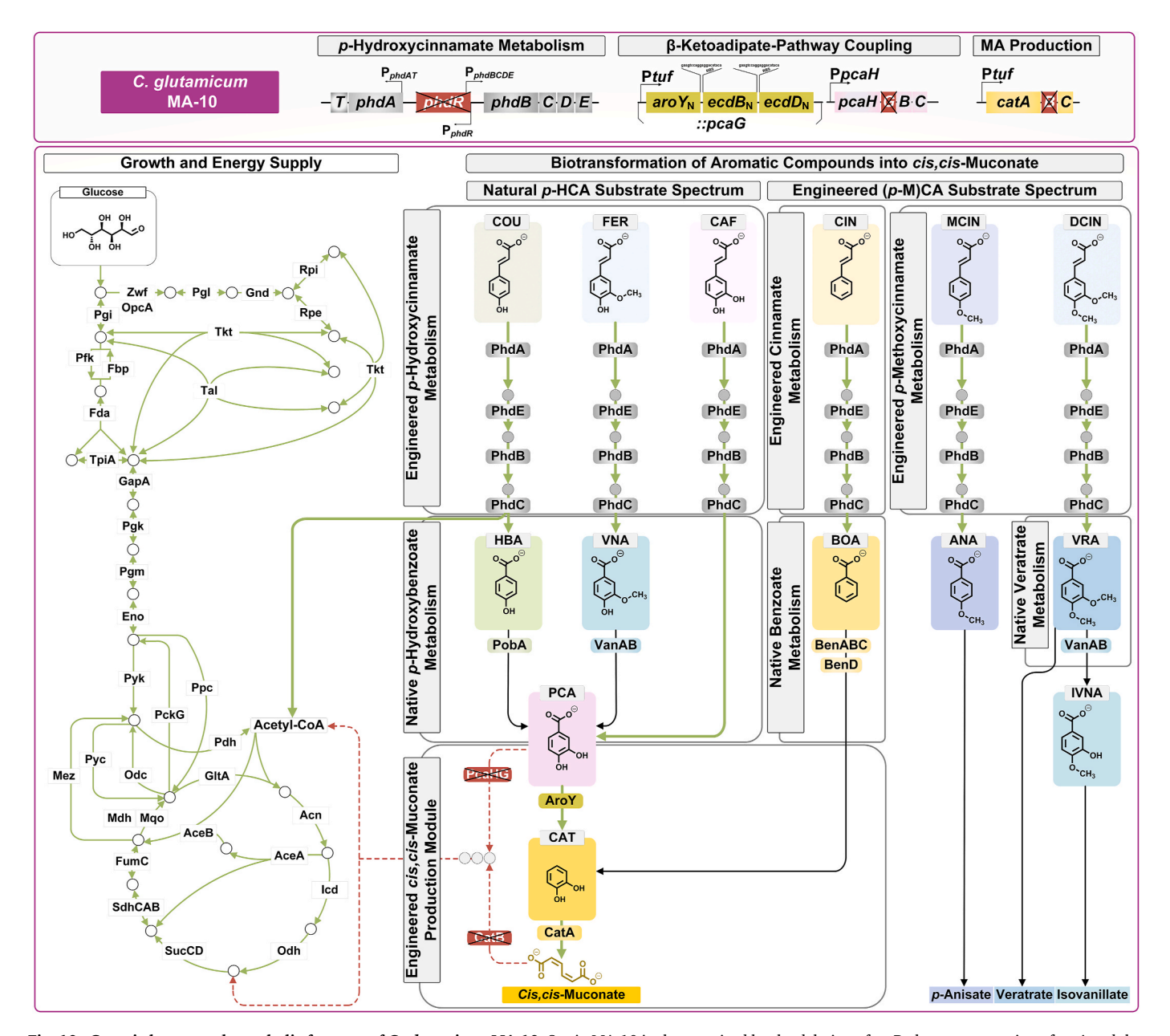


Fig. 10. Genetic layout and metabolic features of *G. glutamicum* **MA-10.** Strain MA-10 is characterized by the deletion of *catB*, the overexpression of *catA* and the coupling of protocatechuate metabolism to *cis, cis-*muconate production by the introduction of the heterologous protocatechuate decarboxylase *aroY*, as well as *ecdB* and *ecdD*, from *E. cloacae* into *pcaG*. Additionally, it carries a deletion of the transcriptional repressor *phdR*, enabling the co-consumption of *p*-hydroxycinnamates and glucose by overcoming the native repression of the *phd* operon in the copresence of glucose. In addition to the natural metabolism of *p*-hydroxycinnamates, the engineered mutant strain MA-10 also metabolizes cinnamate and *p*-methoxycinnamates, which naturally do not belong to the substrate spectrum of *C. glutamicum*. The *p*-methoxybenzoate derivatives resulting from *p*-methoxycinnamate metabolism accumulate as dead-end metabolites, where the conversion of veratrate into isovanillate is catalyzed by native vanillate-*O*-demethylase, as verified in the MA-10-based *vanAB*-deletion mutant, designated MA-11. Activated reactions are depicted as thick, green lines. Deleted reactions are depicted as red dashed lines.

Supplementary File 1), thus revealing that native veratrate metabolism in *C. glutamicum* is mediated by vanillate-*O*-demethylase (Fig. 10). As isovanillate was obviously not further metabolized, *C. glutamicum* seemingly lacks demethylases with substrate specificity for isovanillate, different to other microbes (Providenti et al., 2006; Wolf et al., 2024).

Unlike the tested p-methoxycinnamates, sinapinate remained unconverted, and no intermediates were detected via HPLC or GC-MS (Fig. 7, Fig. S20, Supplementary File 1). Based on biosensor data (Fig. 3) and the chemical properties of the tested compounds (Fig. S21, Supplementary File 1), the additional substituent on sinapinate interferes not only with the PhdR interaction but also with the binding of other enzymes involved in native p-hydroxycinnamate metabolism in C. glutamicum.

4. Discussion

4.1. Carbon catabolite repression as a central bottleneck in aromatic valorization

C. glutamicum is generally known for its high metabolic versatility, including the cometabolism of various carbon sources, such as different sugars (Baritugo et al., 2018; Görke and Stülke, 2008). Our data reveal that carbon catabolite repression (CCR) drastically limits the efficient utilization of p-coumarate, ferulate, and caffeate in the presence of glucose and thus displays another apparently rare example of CCR in this bacterium (Arndt et al., 2008; Gruteser et al., 2012; Krämer et al., 1990). This repression results in a sequential substrate uptake pattern, where glucose is consumed first, and aromatic uptake begins only after glucose depletion (Fig. 2). Notably, this repression appears to be specific to early pathway intermediates, as downstream degradation products such as p-hydroxybenzoate and vanillate are readily co-consumed (Fig. 2G-I). Additionally, structurally related aromatic aldehydes were co-consumed with glucose (Weiland et al., 2023).

Using mCherry-based fluorescent biosensors targeting the back-toback phd operon promoters (P_{phdAT} and $P_{phdBCDE}$), we observed that glucose suppresses expression of the pathway during exponential growth, with a sharp increase in expression only upon glucose depletion (Fig. 3). Interestingly, $P_{phdBCDE}$ consistently showed higher activity than P_{phdAT} (Fig. 3, Table 2), suggesting a native regulatory bias toward prioritizing downstream pathway reactions—possibly to avoid the accumulation of CoA thioesters. This also appears notable considering reports of toxic effects of p-hydroxycinnamoyl-CoA accumulation (Parke and Ornston, 2004). Moreover, the comparatively lower activity of P_{phdAT} likely prevents excessive substrate uptake, further emphasizing the necessity of tightly controlled gene expression for efficient pathway operation. These findings suggest that CCR is not only a metabolic bottleneck but also a key regulatory feature that shapes the flux through the phd pathway. Additionally, in other aromatic-degrading bacteria, such as P. putida and Acinetobacter baylyi, CCR is involved in the co-utilization of p-hydroxycinnamates with sugars or organic acids (Fischer et al., 2008; Johnson et al., 2017). Thus, native substrate preferences display a key challenge for the application of microbial cell factories in plant biomass valorization, which is apparently also true for C. glutamicum.

4.2. PhdR deletion as a targeted strategy to derepress aromatic pathways and increase MA production

We deleted the *phdR* repressor gene to overcome the metabolic block imposed by CCR, creating strain MA-10. This deletion fully derepressed the *phd* operon, enabling *C. glutamicum* to simultaneously cometabolize glucose and aromatics and dramatically increase MA yields (Fig. 6). Compared with the parental MA-6A strain, MA-10 presented up to 48-fold and 18-fold increases in MA production from *p*-coumarate and ferulate, respectively, and metabolized both substrates within 12 h (Fig. 6A-G). The two substrates are primary components of agricultural

residues and grasses and are therefore a central focus of microbial upgrading efforts (Tramontina et al., 2023; Weiland et al., 2022). The microarray analysis confirmed the strong upregulation of *phd* cluster genes, especially *phdBCDE* (log₂-fold change: 6.7–7.9), confirming the biosensor data (Fig. 3, Table 2). Metabolomics further revealed a 3-fold increase in the intracellular abundance of all CoA intermediates in MA-10 (Fig. 4), along with elevated acetyl-CoA levels, highlighting the connection between aromatic metabolism and central carbon flux.

Targeting local regulators such as PhdR provides a clean, efficient strategy for co-utilization without compromising strain robustness in *C. glutamicum*, offering a broadly applicable route for metabolic engineering across microbial platforms considering the similar regulatory layout of *p*-hydroxycinnamate metabolism in various bacteria (Calisti et al., 2008; Kasai et al., 2012; Otani et al., 2014; Parke and Ornston, 2003). In contrast, the manipulation of the global regulator GlxR has proven challenging in *C. glutamicum* because of its essential role and resulting growth defects (Park et al., 2010; Toyoda et al., 2011).

4.3. Acetyl-CoA-driven cross link between p-hydroxycinnamate degradation and central carbon metabolism

Isotopic tracer studies have emerged as powerful tools for unraveling the complexity of microbial aromatic metabolism, offering precise resolution of metabolic fluxes and substrate assimilation across diverse pathways (Del Cerro et al., 2021; Duran et al., 2024; Varman et al., 2016). In this study, the application of ¹³C-labeling provided critical insights into the metabolism of C. glutamicum strain MA-10 cultured on p-coumarate (as biotransformation substrate) and glucose (as growth substrate). The mutant exhibits a disrupted aromatic catabolism at the level of protocatechuate and MA to funnel aromatics (Fig. 8). The expanded 13C labelling dataset, which included biomass sugars and lipids in addition to standard amino acids (Becker et al., 2009, 2011) and secreted metabolites (Wittmann and Heinzle, 2001; Wittmann et al., 2004b), significantly improved pathway resolution and exposed global redistribution of aromatic carbon within central metabolism. The observed extensive incorporation of unlabeled (12C) carbon from the side chain of p-coumarate into major biomass components not only demonstrates the strain's capacity to metabolize lignin-derived aromatics efficiently but also reveals a comprehensive and previously underappreciated integration of aromatic degradation with core biosynthetic processes—or "division of labor"—between aromatic compound degradation and central metabolism, as also observed in P. putida (Kukurugya et al., 2019). It appears interesting to further study how C. glutamicum mediates the adaptation of its central carbon metabolism with regard to transcriptional and metabolic control (Table 2) (Schilling et al., 2007).

One of the striking findings is the pronounced ¹²C-enrichment in fatty acids and 2-oxoglutarate-derived amino acids, supporting a key role of acetyl-CoA as a metabolic node linking p-coumarate catabolism to biosynthesis. The conversion of side-chain carbons from p-coumarate into acetyl-CoA appears efficient, with subsequent routing into the TCA cycle and anabolic branches, as reflected by labeling in glutamate, proline, and arginine. Further ¹²C-enrichment in oxaloacetate-derived amino acids and nucleotide sugars points to broader participation of aromatic-derived carbon in gluconeogenesis and nucleotide biosynthesis. Notably, evidence for glyoxylate shunt activity—normally repressed by GlxR in the presence of glucose (Kim et al., 2004)—suggests carbon conservation through bypassing decarboxylation steps, similar to cells grown on mixtures of glucose and acetate (Wendisch et al., 2000). Although C. glutamicum is a well-established aromatic degrader, the global regulatory mechanisms governing aromatic catabolism—particularly in the context of mixed substrates—remain incompletely understood. For instance, GlxR has been implicated in the metabolism of protocatechuate (Haussmann and Poetsch, 2012), vanillate (Morabbi Heravi et al., 2015), gentisate, and 3-hydroxybenzoate (Kim et al., 2004), and p-hydroxycinnamates (this work).

The detection of unlabeled carbon in sugars typically derived from glycolytic and pentose phosphate intermediates implied that aromatic substrates alone support complete biosynthetic demands. The ability of MA-10 to produce MA solely from *p*-coumarate (Fig. 8B) further demonstrates its potential for lignin valorization from grassy biomass without additional sugar carbon, an important steps towards economic efficiency (Sonoki et al., 2018). Together, these findings position strain MA-10 as a highly effective chassis for lignin valorization. Future work should focus on harnessing and engineering the metabolic integration between aromatics catabolism and central metabolism to optimize carbon flux, enhance yields of target products, and expand the range of useable aromatic substrates.

4.4. Substrate spectrum expansion and new pathways for lignin-derived compounds

In addition to performance improvements, strain MA-10 displayed a remarkably broadened substrate range, including a newly acquired metabolic capability for methoxylated cinnamates such as 4-methoxycinnamate and 3,4-dimethoxycinnamate (Fig. 10). These substrates, which were previously unutilized by *C. glutamicum*, were partially degraded into novel benzoate derivatives such as anisate and veratrate—compounds with potential applications in cosmetics and pharmaceuticals. (Czarnecka et al., 2018; Durairaj et al., 2023; Martins and Marto, 2023). MA-10 also degraded cinnamate—a capability not observed in the wild-type or MA-6A strains—through its conversion to benzoate and MA, resulting in the activation of native but previously silent degradation pathways (Fig. 10). The deletion of *vanAB*, encoding vanillate-*O*-demethylase, confirmed the pathway leading to veratrate demethylation into isovanillate, which accumulated as a dead-end product (Fig. S18 and 19, Supplementary File 1).

Considering the biosensor data (Fig. 3), along with the expanded substrate spectrum observed in C. glutamicum MA-10 (Fig. 7), it appears that the organism's ability to convert structurally related cinnamates is primarily limited by the substrate specificity of the transcriptional regulator PhdR. Repression by PhdR seems to be relieved only in the presence of aromatic compounds that feature both a propenoic acid side chain (-CH=CH-COOH) plus a hydroxyl group in the para-position of the aromatic ring (Fig. 7). Notably, the para-hydroxyl group has been implicated in forming hydrogen bonds during ligand interactions with other MarR-type repressors involved in p-hydroxycinnamate catabolism (Kim et al., 2016; Otani et al., 2016). Interestingly, other enzymes in the phd pathway appear to tolerate alternative para-substituents. Removal of the phdR repressor was therefore key to broadening the substrate spectrum, revealing that the downstream enzymes of the phd pathway are inherently more flexible in substrate acceptance than previously assumed (Kallscheuer et al., 2016).

This extended substrate flexibility is crucial for lignocellulose valorization, when targeting a holistic valorization of diverse agricultural and food processing residues. Notably, even though caffeate is generally less abundant in agricultural residues than coumarate and ferulate, there are some notable exceptions that deserve attention. In rice straw, caffeate has been reported as the major phenolic compound (Karimi et al., 2014). Additionally, caffeate is significantly present in various agro-industrial byproducts such as soybean meal (Oskoueian et al., 2011), spent coffee grounds (Angeloni et al., 2020), and sorghum straw (Qian et al., 2024). In addition, the different p-methoxylated cinnamates, converted by the genetically-engineered strain MA-10 have been reported to occur in lignocellulosics (Jönsson and Martín, 2016; Zhang et al., 2020). Considering the increasing interest in cinnamate derivatives and related attempts to increase their isolation and production (Fonseca et al., 2019), our findings position C. glutamicum MA-10 as a promising platform for broad-spectrum aromatic upgrading, especially in the context of mixed-substrate lignin hydrolysates.

5. Summary and outlook

In this work, C. glutamicum was successfully engineered for the increased metabolism of different p-hydroxycinnamates and cinnamates. In the first step, carbon catabolite repression was identified as a major bottleneck for the conversion of these aromatics into MA in the presence of glucose, which was alleviated by deletion of the local regulator PhdR. The novel producer strain MA-10, with a deregulated phd operon, cometabolized different p-hydroxycinnamates together with glucose, leading to overall improved MA production from elevated concentrations of the provided aromatic biotransformation substrates. The performance gains were underpinned by mechanistic insights from transcriptomic, metabolomic, and ¹³C-isotopic labeling analyses. These revealed a substantial increase in the intracellular abundance of CoA thioesters and acetyl-CoA, highlighting a tight metabolic cross-link between aromatic catabolism and central carbon metabolism. Isotopic tracer experiments further confirmed that side-chain carbons from pcoumarate significantly contribute to biomass precursors via acetyl-CoA. Enrichment of ¹²C in fatty acids, amino acids, nucleotide sugars, and cell wall components indicated global carbon redistribution, involving key metabolic pathways such as the TCA cycle, glyoxylate shunt, and gluconeogenesis. Importantly, this redistribution enabled sugar-free MA production from p-coumarate as the sole carbon and energy source—providing a proof-of-concept for fully aromatic-driven growth and biosynthesis.

Beyond improving MA titers and yields, *phdR* deletion also expanded the metabolic range of *C. glutamicum* to include non-native substrates. Strain MA-10 gained degraded methoxylated cinnamates—such as 4-methoxycinnamate and 3,4-dimethoxycinnamate—into novel benzoate derivatives and could metabolize cinnamate into MA via the benzoate pathway. These capabilities were not present in the wild-type or earlier engineered strains and demonstrate how relieving native regulatory constraints can activate latent metabolic functions. The strain also efficiently processed straw-derived lignin hydrolysates, confirming its suitability for real-world lignin valorization. This work positions *C. glutamicum* MA-10 as a promising platform for broad-spectrum aromatic upgrading. Future developments should focus on optimizing carbon flux, expanding substrate utilization, and adapting the strain for industrial bioprocesses using complex lignin streams.

CRediT authorship contribution statement

Fabia Weiland: Writing – review & editing, Writing – original draft, Visualization, Validation, Methodology, Investigation, Formal analysis, Data curation, Conceptualization. Kyoyoung Seo: Writing – review & editing, Validation, Methodology, Investigation, Formal analysis. Franka Janz: Writing – review & editing, Validation, Methodology, Investigation, Formal analysis. Marius Grad: Writing – review & editing, Validation, Methodology, Investigation, Formal analysis. Lea Geldmacher: Writing – review & editing, Validation, Methodology, Investigation, Formal analysis. Lea deliting, Validation, Formal analysis. Michael Kohlstedt: Writing – review & editing, Validation, Methodology, Investigation, Formal analysis, Data curation. Judith Becker: Conceptualization, Methodology, Supervision. Christoph Wittmann: Writing – review & editing, Writing – original draft, Visualization, Validation, Supervision, Resources, Project administration, Methodology, Funding acquisition, Formal analysis, Conceptualization.

Declaration of competing interests

The authors have filed patent applications on the use of lignin for bioproduction.

Acknowledgments

This project has received funding from the European Union's

Horizon Europe Program under Grant Agreement number: 101057971. Christoph Wittmann acknowledges support from the German Ministry for Education and Research (BMBF) through the grant STRAW2HEALTH (FKZ 031B1570A). Fabia Weiland thanks the HaVo Foundation, Ludwigshafen, Germany, for funding her through a doctoral fellowship. Judith Becker, Fabia Weiland, and Michael Kohlstedt acknowledge support through young investigator awards sponsored by the Hans-and-Ruth-Giessen Foundation, St. Ingbert, Germany. The authors acknowledge the excellent assistance of Adrian Gleissner (Systems Biotechnology, Saarland University) for lignin depolymerization.

Appendix A. Supplementary data

Supplementary data to this article can be found online at https://doi.org/10.1016/j.ymben.2025.08.004.

Data availability

Data will be made available on request.

References

- Adler, P., Bolten, C.J., Dohnt, K., Hansen, C.E., Wittmann, C., 2013. Core fluxome and metafluxome of lactic acid bacteria under simulated cocoa pulp fermentation conditions. Appl. Environ. Microbiol. 79, 5670–5681.
- Andrade, M.C., Gorgulho Silva, C.d.O., de Souza Moreira, L.R., Ferreira Filho, E.X., 2021.
 Crop residues: applications of lignocellulosic biomass in the context of a biorefinery.
 Front. Energy 1–22.
- Angeloni, S., Nzekoue, F.K., Navarini, L., Sagratini, G., Torregiani, E., Vittori, S., Caprioli, G., 2020. An analytical method for the simultaneous quantification of 30 bioactive compounds in spent coffee ground by HPLC-MS/MS. J. Mass Spectrom. 55, e4519
- Arndt, A., Auchter, M., Ishige, T., Wendisch, V.F., Eikmanns, B.J., 2008. Ethanol catabolism in Corynebacterium glutamicum. J. Mol. Microbiol. Biotechnol. 15, 222–233.
- Baritugo, K.-A., Kim, H.T., David, Y., Choi, J.-i., Hong, S.H., Jeong, K.J., Choi, J.H., Joo, J.C., Park, S.J., 2018. Metabolic engineering of Corynebacterium glutamicum for fermentative production of chemicals in biorefinery. Appl. Microbiol. Biotechnol. 102, 3915–3937.
- Becker, J., Buschke, N., Bücker, R., Wittmann, C., 2010. Systems Level Engineering of Corynebacterium glutamicum–reprogramming Translational Efficiency for Superior Production, vol. 10. Engineering in life sciences, pp. 430–438.
- Becker, J., Klopprogge, C., Schröder, H., Wittmann, C., 2009. Metabolic engineering of the tricarboxylic acid cycle for improved lysine production by *Corynebacterium glutamicum*. Appl. Environ. Microbiol. 75, 7866–7869.
- Becker, J., Klopprogge, C., Zelder, O., Heinzle, E., Wittmann, C., 2005. Amplified expression of fructose 1,6-bisphosphatase in *Corynebacterium glutamicum* increases in vivo flux through the pentose phosphate pathway and lysine production on different carbon sources. Appl. Environ. Microbiol. 71, 8587–8596.
- Becker, J., Kuhl, M., Kohlstedt, M., Starck, S., Wittmann, C., 2018a. Metabolic engineering of *Corynebacterium glutamicum* for the production of *cis*, *cis*-muconic acid from lignin. Microb. Cell Fact. 17, 115.
- Becker, J., Rohles, C.M., Wittmann, C., 2018b. Metabolically engineered Corynebacterium glutamicum for bio-based production of chemicals, fuels, materials, and healthcare products. Metab. Eng. 50, 122–141.
- Becker, J., Wittmann, C., 2012. Bio-based production of chemicals, materials and fuelscorynebacterium glutamicum as versatile cell factory. Curr. Opin. Biotechnol. 23, 621-640.
- Becker, J., Wittmann, C., 2019. A field of dreams: lignin valorization into chemicals, materials, fuels, and health-care products. Biotechnol. Adv. 37, 107360.
- Becker, J., Zelder, O., Hafner, S., Schroder, H., Wittmann, C., 2011. From zero to herodesign-based systems metabolic engineering of *Corynebacterium glutamicum* for Llysine production. Metab. Eng. 13, 159–168.
- Beganovic, S., Rückert-Reed, C., Sucipto, H., Shu, W., Glaser, L., Patschkowski, T., Struck, B., Kalinowski, J., Luzhetskyy, A., Wittmann, C., 2023. Systems biology of industrial oxytetracycline production in *Streptomyces rimosus*: the secrets of a mutagenized hyperproducer. Microb. Cell Fact. 22, 222.
- Bichot, A., Delgenes, J.-P., Méchin, V., Carrère, H., Bernet, N., García-Bernet, D., 2018. Understanding biomass recalcitrance in grasses for their efficient utilization as biorefinery feedstock. Rev. Environ. Sci. Biotechnol. 17, 707–748.
- Bugg, T.D.H., Williamson, J.J., Alberti, F., 2021. Microbial hosts for metabolic engineering of lignin bioconversion to renewable chemicals. Renew Sust Energ Rev 152, 111674.
- Cachet, N., Camy, S., Benjelloun-Mlayah, B., Condoret, J.-S., Delmas, M., 2014. Esterification of organosolv lignin under supercritical conditions. Ind. Crop. Prod. 58, 287–297.
- Calisti, C., Ficca, A.G., Barghini, P., Ruzzi, M., 2008. Regulation of ferulic catabolic genes in Pseudomonas fluorescens BF13: involvement of a MarR family regulator. Appl. Microbiol. Biotechnol. 80, 475–483.

- Cecil, J.H., Garcia, D.C., Giannone, R.J., Michener, J.K., 2018. Rapid, parallel identification of catabolism pathways of lignin-derived aromatic compounds in Novosphingobium aromaticivorans. Appl. Environ. Microbiol. 84 (18), e01185.
- Chao, H., Zhou, N.-Y., 2014. Involvement of the global regulator GlxR in 3-hydroxybenzoate and gentisate utilization by Corynebacterium glutamicum. Appl. Environ. Microbiol. 80, 4215–4225.
- Christmann, J., Cao, P., Becker, J., Desiderato, C.K., Goldbeck, O., Riedel, C.U., Kohlstedt, M., Wittmann, C., 2023. High-efficiency production of the antimicrobial peptide pediocin PA-1 in metabolically engineered Corynebacterium glutamicum using a microaerobic process at acidic pH and elevated levels of bivalent calcium ions. Microb. Cell Fact. 22, 41.
- Corona, A., Biddy, M.J., Vardon, D.R., Birkved, M., Hauschild, M.Z., Beckham, G.T., 2018. Life cycle assessment of adipic acid production from lignin. Green Chem. 20, 3857–3866.
- Czarnecka, M., Świtalska, M., Wietrzyk, J., Maciejewska, G., Gliszczyńska, A., 2018.
 Synthesis, characterization, and in vitro cancer cell growth inhibition evaluation of novel phosphatidylcholines with anisic and veratric acids. Molecules 23, 2022.
- Del Cerro, C., Erickson, E., Dong, T., Wong, A.R., Eder, E.K., Purvine, S.O., Mitchell, H.D., Weitz, K.K., Markillie, L.M., Burnet, M.C., Hoyt, D.W., Chu, R.K., Cheng, J.F., Ramirez, K.J., Katahira, R., Xiong, W., Himmel, M.E., Subramanian, V., Linger, J.G., Salvachua, D., 2021. Intracellular pathways for lignin catabolism in white-rot fungi. Proc. Natl. Acad. Sci. U. S. A. 118.
- Dietrich, D., Jovanovic Gasovic, S., Cao, P., Kohlstedt, M., Wittmann, C., 2023. Refactoring the architecture of a polyketide gene cluster enhances docosahexaenoic acid production in *Yarrowia lipolytica* through improved expression and genetic stability. Microb. Cell Fact. 22, 199.
- Dolan, S.K., Wijaya, A., Kohlstedt, M., Gläser, L., Brear, P., Silva-Rocha, R., Wittmann, C., Welch, M., 2022. Systems-wide dissection of organic acid assimilation in *Pseudomonas aeruginosa* reveals a novel path to underground metabolism. mBio 13, e0254122.
- Durairaj, K., Balasubramanian, B., Arumugam, V.A., Easwaran, M., Park, S., Issara, U., Pushparaj, K., Al-Dhabi, N.A., Arasu, M.V., Liu, W.-C., 2023. Biocompatibility of veratric acid-encapsulated chitosan/methylcellulose hydrogel: biological characterization, osteogenic efficiency with in silico molecular modeling. Appl. Biochem. Biotechnol. 195, 4429–4446.
- Duran, K., Kohlstedt, M., van Erven, G., Klostermann, C.E., America, A.H.P., Bakx, E., Baars, J.J.P., Gorissen, A., de Visser, R., de Vries, R.P., Wittmann, C., Comans, R.N.J., Kuyper, T.W., Kabel, M.A., 2024. From ¹³C-lignin to ¹³C-mycelium: *Agaricus bisporus* uses polymeric lignin as a carbon source. Sci. Adv. 10, eadl3419.
- FAO, F. a. A. O. o. t. U. N., 2022. Establishing residue supply chains to reduce open burning. The Case of Rice Straw and Renewable Energy in Punjab, India, Environment and Natural Resources Management Working Paper No. 95.
- Fischer, R., Bleichrodt, F.S., Gerischer, U.C., 2008. Aromatic degradative pathways in Acinetobacter baylyi underlie carbon catabolite repression. Microbiology 154, 3095–3103.
- Fonseca, A.C., Lima, M.S., Sousa, A.F., Silvestre, A.J., Coelho, J.F., Serra, A.C., 2019. Cinnamic acid derivatives as promising building blocks for advanced polymers: synthesis, properties and applications. Polym. Chem. 10, 1696–1723.
- Gläser, L., Kuhl, M., Jovanovic, S., Fritz, M., Vogeli, B., Erb, T.J., Becker, J., Wittmann, C., 2020. A common approach for absolute quantification of short chain CoA thioesters in prokaryotic and eukaryotic microbes. Microb. Cell Fact. 19, 160.
- Gläser, L., Kuhl, M., Stegmüller, J., Rückert, C., Myronovskyi, M., Kalinowski, J., Luzhetskyy, A., Wittmann, C., 2021. Superior production of heavy pamamycin derivatives using a bkdR deletion mutant of *Streptomyces albus* J1074/R2. Microb. Cell Fact, 20, 111.
- Gonçalves, C.C., Bruce, T., Silva, C.d.O.G., Fillho, E.X.F., Noronha, E.F., Carlquist, M., Parachin, N.S., 2020. Bioprospecting microbial diversity for lignin valorization: dry and wet screening methods. Front. Microbiol. 11, 1081.
- Görke, B., Stülke, J., 2008. Carbon catabolite repression in bacteria: many ways to make the most out of nutrients. Nat. Rev. Microbiol. 6, 613–624.
- Gruteser, N., Marin, K., Krämer, R., Thomas, G.H., 2012. Sialic acid utilization by the soil bacterium Corynebacterium glutamicum. FEMS Microbiol. Lett. 336, 131–138.
- Hatfield, R.D., Rancour, D.M., Marita, J.M., 2017. Grass cell walls: a story of cross-linking. Front. Plant Sci. 7, 2056.
- Haussmann, U., Poetsch, A., 2012. Global proteome survey of protocatechuate- and glucose-grown Corynebacterium glutamicum reveals multiple physiological differences. J. Proteonomics 75, 2649–2659.
- Hoffmann, S.L., Jungmann, L., Schiefelbein, S., Peyriga, L., Cahoreau, E., Portais, J.C., Becker, J., Wittmann, C., 2018. Lysine production from the sugar alcohol mannitod: design of the cell factory Corynebacterium glutamicum SEA-3 through integrated analysis and engineering of metabolic pathway fluxes. Metab. Eng. 47, 475–487.
- Jiang, K., Li, L., Long, L., Ding, S., 2016. Comparison of alkali treatments for efficient release of p-coumaric acid and enzymatic saccharification of sorghum pith. Bioresour. Technol. 207, 1–10.
- Johnson, C.W., Abraham, P.E., Linger, J.G., Khanna, P., Hettich, R.L., Beckham, G.T., 2017. Eliminating a global regulator of carbon catabolite repression enhances the conversion of aromatic lignin monomers to muconate in *Pseudomonas putida* KT2440. Metab Eng Commun 5, 19–25.
- Jönsson, L.J., Martín, C., 2016. Pretreatment of lignocellulose: formation of inhibitory by-products and strategies for minimizing their effects. Bioresour. Technol. 199, 103–112.
- Jovanovic Gasovic, S., Dietrich, D., Gläser, L., Cao, P., Kohlstedt, M., Wittmann, C., 2023. Multi-omics view of recombinant *Yarrowia lipolytica*: enhanced ketogenic amino acid catabolism increases polyketide-synthase-driven docosahexaenoic production to high selectivity at the gram scale. Metab. Eng. 80, 45–65.

- Kallscheuer, N., Vogt, M., Kappelmann, J., Krumbach, K., Noack, S., Bott, M., Marienhagen, J., 2016. Identification of the phd gene cluster responsible for phenylpropanoid utilization in Corynebacterium glutamicum. Appl. Microbiol. Biotechnol. 100, 1871–1881.
- Karimi, E., Mehrabanjoubani, P., Keshavarzian, M., Oskoueian, E., Jaafar, H.Z., Abdolzadeh, A., 2014. Identification and quantification of phenolic and flavonoid components in straw and seed husk of some rice varieties (Oryza sativa L.) and their antioxidant properties. J. Sci. Food Agric. 94, 2324–2330.
- Karp, E.M., Nimlos, C.T., Deutch, S., Salvachúa, D., Cywar, R.M., Beckham, G.T., 2016.
 Quantification of acidic compounds in complex biomass-derived streams. Green Chem. 18, 4750–4760.
- Kasai, D., Kamimura, N., Tani, K., Umeda, S., Abe, T., Fukuda, M., Masai, E., 2012. Characterization of FerC, a MarR-type transcriptional regulator, involved in transcriptional regulation of the ferulate catabolic operon in Sphingobium sp. strain SYK-6. FEMS Microbiol. Lett. 332 (1), 68–75.
- Katahira, R., Mittal, A., McKinney, K., Chen, X., Tucker, M.P., Johnson, D.K., Beckham, G.T., 2016. Base-catalyzed depolymerization of biorefinery lignins. ACS Sustain. Chem. Eng. 4, 1474–1486.
- Kiefer, P., Heinzle, E., Zelder, O., Wittmann, C., 2004. Comparative metabolic flux analysis of lysine-producing *Corynebacterium glutamicum* cultured on glucose or fructose. Appl. Environ. Microbiol. 70, 229–239.
- Kim, H.J., Kim, T.H., Kim, Y., Lee, H.S., 2004. Identification and characterization of glxR, a gene involved in regulation of glyoxylate bypass in *Corynebacterium glutamicum*. J. Bacteriol. 186, 3453–3460.
- Kim, Y., Joachimiak, G., Bigelow, L., Babnigg, G., Joachimiak, A., 2016. How aromatic compounds block DNA binding of HcaR catabolite regulator. J. Biol. Chem. 291, 13243–13256.
- Kind, S., Jeong, W.K., Schröder, H., Wittmann, C., 2010. Systems-wide metabolic pathway engineering in Corynebacterium glutamicum for bio-based production of diaminopentane. Metab. Eng. 12, 341–351.
- Kohl, T.A., Tauch, A., 2009. The GlxR regulon of the amino acid producer Corynebacterium glutamicum: detection of the corynebacterial core regulon and integration into the transcriptional regulatory network model. J. Biotechnol. 143, 239–246.
- Kohlstedt, M., Starck, S., Barton, N., Stolzenberger, J., Selzer, M., Mehlmann, K., Schneider, R., Pleissner, D., Rinkel, J., Dickschat, J.S., Venus, J., J, B.J. H.v.D., Wittmann, C., 2018. From lignin to nylon: cascaded chemical and biochemical conversion using metabolically engineered *Pseudomonas putida*. Metab. Eng. 47, 279–293
- Kohlstedt, M., Weimer, A., Weiland, F., Stolzenberger, J., Selzer, M., Sanz, M., Kramps, L., Wittmann, C., 2022. Biobased PET from lignin using an engineered cis, cis-muconate-producing *Pseudomonas putida* strain with superior robustness, energy and redox properties. Metab. Eng. 72, 337–352.
- Kohlstedt, M., Wittmann, C., 2019. GC-MS-based C-13 metabolic flux analysis resolves the parallel and cyclic glucose metabolism of *Pseudomonas putida* KT2440 and *Pseudomonas aeruginosa* PAO1. Metab. Eng. 54, 35–53.
- Korneli, C., Biedendieck, R., David, F., Jahn, D., Wittmann, C., 2013. High yield production of extracellular recombinant levansucrase by Bacillus megaterium. Appl. Microbiol. Biotechnol. 97, 3343–3353.
- Krämer, R., Lambert, C., Hoischen, C., Ebbighausen, H., 1990. Uptake of glutamate in Corynebacterium glutamicum: 1. Kinetic properties and regulation by internal pH and potassium. Eur. J. Biochem. 194, 929–935.
- Kuatsjah, E., Johnson, C.W., Salvachúa, D., Werner, A.Z., Zahn, M., Szostkiewicz, C.J., Singer, C.A., Dominick, G., Okekeogbu, I., Haugen, S.J., Woodworth, S.P., Ramirez, K.J., Giannone, R.J., Hettich, R.L., McGeehan, J.E., Beckham, G.T., 2022. Debottlenecking 4-hydroxybenzoate hydroxylation in Pseudomonas putida KT2440 improves muconate productivity from p-coumarate. Metab. Eng. 70, 31–42.
- Kuhl, M., Glaser, L., Rebets, Y., Ruckert, C., Sarkar, N., Hartsch, T., Kalinowski, J., Luzhetskyy, A., Wittmann, C., 2020. Microparticles globally reprogram Streptomyces albus toward accelerated morphogenesis, streamlined carbon core metabolism, and enhanced production of the antituberculosis polyketide pamamycin. Biotechnol. Bioeng. 117, 3858–3875.
- Kukurugya, M.A., Mendonca, C.M., Solhtalab, M., Wilkes, R.A., Thannhauser, T.W., Aristilde, L., 2019. Multi-omics analysis unravels a segregated metabolic flux network that tunes co-utilization of sugar and aromatic carbons in Pseudomonas putida. J. Biol. Chem. 294, 8464–8479.
- Li, M.H., Li, H., Zhang, X., Liang, Y.C., Li, C., Sun, M.L., Li, K., Liu, C.G., Sinskey, A.J., 2024. Metabolic engineering of Corynebacterium glutamicum: unlocking its potential as a key cell factory platform for organic acid production. Biotechnol. Adv. 77, 108475.
- Liu, A., Ellis, D., Mhatre, A., Brahmankar, S., Seto, J., Nielsen, D.R., Varman, A.M., 2024. Biomanufacturing of value-added chemicals from lignin. Curr. Opin. Biotechnol. 89, 103178.
- Martins, A.M., Marto, J.M., 2023. A sustainable life cycle for cosmetics: from design and development to post-use phase. Sustain. Chem. Pharm. 35, 101178.
- Mokwatlo, S.C., Klein, B.C., Benavides, P.T., Tan, E.C.D., Kneucker, C.M., Ling, C., Singer, C.A., Lyons, R., Sànchez i Nogué, V., Hestmark, K.V., Ingraham, M.A., Ramirez, K.J., Johnson, C.W., Beckham, G.T., Salvachúa, D., 2024. Bioprocess development and scale-up for cis,cis-muconic acid production from glucose and xylose by Pseudomonas putida. Green Chem. 26, 10152–10167.
- Morabbi Heravi, K., Lange, J., Watzlawick, H., Kalinowski, J., Altenbuchner, J., 2015. Transcriptional regulation of the vanillate utilization genes (vanABK Operon) of Corynebacterium glutamicum by VanR, a PadR-like repressor. J. Bacteriol. 197, 959–972.
- Oskoueian, E., Abdullah, N., Hendra, R., Karimi, E., 2011. Bioactive compounds, antioxidant, xanthine oxidase inhibitory, tyrosinase inhibitory and anti-

- inflammatory activities of selected agro-industrial by-products. Int. J. Mol. Sci. 12, 8610-8625
- Otani, H., Lee, Y.-E., Casabon, I., Eltis, L.D., 2014. Characterization of phydroxycinnamate catabolism in a soil Actinobacterium. J. Bacteriol. 196, 4293–4303.
- Otani, H., Stogios, P.J., Xu, X., Nocek, B., Li, S.N., Savchenko, A., Eltis, L.D., 2016. The activity of CouR, a MarR family transcriptional regulator, is modulated through a novel molecular mechanism. Nucleic Acids Res. 44 (2), 595–607.
- Ou, S., Luo, Y., Huang, C., Jackson, M., 2009. Production of coumaric acid from sugarcane bagasse. Innov. Food Sci. Emerg. Technol. 10, 253–259.
- Park, S.-Y., Moon, M.-W., Subhadra, B., Lee, J.-K., 2010. Functional characterization of the glxR deletion mutant of Corynebacterium glutamicum ATCC 13032: involvement of GlxR in acetate metabolism and carbon catabolite repression. FEMS Microbiol. Lett. 304, 107–115.
- Parke, D., Ornston, L.N., 2003. Hydroxycinnamate (hca) catabolic genes from Acinetobacter sp. strain ADP1 are repressed by HcaR and are induced by hydroxycinnamoyl-coenzyme A thioesters. Appl. Environ. Microbiol. 69, 5308, 5400
- Parke, D., Ornston, L.N., 2004. Toxicity caused by hydroxycinnamoyl-coenzyme A thioester accumulation in mutants of Acinetobacter sp. strain ADP1. Appl. Environ. Microbiol. 70, 2974–2983.
- Pauli, S., Kohlstedt, M., Lamber, J., Weiland, F., Becker, J., Wittmann, C., 2023. Systems metabolic engineering upgrades Corynebacterium glutamicum for selective highlevel production of the chiral drug precursor and cell-protective extremolyte Lpipecolic acid. Metab. Eng. 77, 100–117.
- Peracchi, L.M., Panahabadi, R., Barros-Rios, J., Bartley, L.E., Sanguinet, K.A., 2024. Grass lignin: biosynthesis, biological roles, and industrial applications. Front. Plant Sci. 15, 1343097.
- Providenti, M.A., O'Brien, J.M., Ruff, J.r., Cook, A.M., Lambert, I.B., 2006. Metabolism of isovanillate, vanillate, and veratrate by Comamonas testosteroni strain BR6020.

 J. Bacteriol. 188, 3862–3869.
- Qian, S., Lu, M., Zhou, X., Sun, S., Han, Z., Song, H., 2024. Improvement in caffeic acid and ferulic acid extraction by oscillation-assisted mild hydrothermal pretreatment from sorghum straws. Bioresour. Technol. 396, 130442.
- Rautengarten, C., Baidoo, E., Keasling, J.D., Scheller, H.V., 2010. A simple method for enzymatic synthesis of unlabeled and radiolabeled hydroxycinnamate-CoA. BioEnergy Research 3, 115–122.
- Rodriguez, A., Salvachúa, D., Katahira, R., Black, B.A., Cleveland, N.S., Reed, M., Smith, H., Baidoo, E.E., Keasling, J.D., Simmons, B.A., 2017. Base-catalyzed depolymerization of solid lignin-rich streams enables microbial conversion. ACS Sustain. Chem. Eng. 5, 8171–8180.
- Rohles, C., Pauli, S., Gießelmann, G., Kohlstedt, M., Becker, J., Wittmann, C., 2022. Systems metabolic engineering of Corynebacterium glutamicum eliminates all by-products for selective and high-yield production of the platform chemical 5-aminovalerate. Metab. Eng. 73, 168–181.
- Rohles, C.M., Gießelmann, G., Kohlstedt, M., Wittmann, C., Becker, J., 2016. Systems metabolic engineering of Corynebacterium glutamicum for the production of the carbon-5 platform chemicals 5-aminovalerate and glutarate. Microb. Cell Fact. 15, 1–13.
- Salvachua, D., Johnson, C.W., Singer, C.A., Rohrer, H., Peterson, D.J., Black, B.A., Knapp, A., Beckham, G.T., 2018. Bioprocess development for muconic acid production from aromatic compounds and lignin. Green Chem. 20, 5007–5019.
- Schilling, O., Frick, O., Herzberg, C., Ehrenreich, A., Heinzle, E., Wittmann, C., Stulke, J., 2007. Transcriptional and metabolic responses of *Bacillus subtilis* to the availability of organic acids: transcription regulation is important but not sufficient to account for metabolic adaptation. Appl. Environ. Microbiol. 73, 499–507.
- Schröder, J., Tauch, A., 2010. Transcriptional regulation of gene expression in Corynebacterium glutamicum: the role of global, master and local regulators in the modular and hierarchical gene regulatory network. FEMS Microbiol. Rev. 34 (5), 685–737
- Schulze, D., Kohlstedt, M., Becker, J., Cahoreau, E., Peyriga, L., Makowka, A.,
 Hildebrandt, S., Gutekunst, K., Portais, J.C., Wittmann, C., 2022. GC/MS-based (13)
 C metabolic flux analysis resolves the parallel and cyclic photomixotrophic
 metabolism of *Synechocystis* sp. PCC 6803 and selected deletion mutants including
 the Entner-Doudoroff and phosphoketolase pathways. Microb. Cell Fact. 21, 69.
- Schwechheimer, S.K., Becker, J., Peyriga, L., Portais, J.C., Sauer, D., Muller, R., Hoff, B., Haefner, S., Schroder, H., Zelder, O., Wittmann, C., 2018a. Improved riboflavin production with Ashbya gossypii from vegetable oil based on (13)C metabolic network analysis with combined labeling analysis by GC/MS, LC/MS, 1D, and 2D NMR. Metab. Eng. 47, 357–373.
- Schwechheimer, S.K., Becker, J., Peyriga, L., Portais, J.C., Wittmann, C., 2018b. Metabolic flux analysis in *Ashbya gossypii* using (13)C-labeled yeast extract: industrial riboflavin production under complex nutrient conditions. Microb. Cell Fact. 17, 162.
- Seo, K., Shu, W., Rückert-Reed, C., Gerlinger, P., Erb, T.J., Kalinowski, J., Wittmann, C., 2023. From waste to health-supporting molecules: biosynthesis of natural products from lignin-, plastic- and seaweed-based monomers using metabolically engineered Streptomyces lividans. Microb. Cell Fact. 22, 262.
- Sonoki, T., Takahashi, K., Sugita, H., Hatamura, M., Azuma, Y., Sato, T., Suzuki, S., Kamimura, N., Masai, E., 2018. Glucose-free cis,cis-muconic acid production via new metabolic designs corresponding to the heterogeneity of lignin. ACS Sustain. Chem. Eng. 6, 1256–1264.
- Torre, P., Aliakbarian, B., Rivas, B., Domínguez, J.M., Converti, A., 2008. Release of ferulic acid from corn cobs by alkaline hydrolysis. Biochem. Eng. J. 40, 500–506.
- Toyoda, K., Teramoto, H., Inui, M., Yukawa, H., 2009a. The ldhA gene, encoding fermentative L-lactate dehydrogenase of Corynebacterium glutamicum, is under the

- control of positive feedback regulation mediated by LldR. J. Bacteriol. 191, 4251–4258.
- Toyoda, K., Teramoto, H., Inui, M., Yukawa, H., 2009b. Molecular mechanism of SugR-mediated sugar-dependent expression of the *ldhA* gene encoding L-lactate dehydrogenase in *Corynebacterium glutamicum*. Appl. Microbiol. Biotechnol. 83, 315–327
- Toyoda, K., Teramoto, H., Inui, M., Yukawa, H., 2011. Genome-wide identification of in vivo binding sites of GlxR, a cyclic AMP receptor protein-type regulator in Corynebacterium glutamicum. J. Bacteriol. 193, 4123–4133.
- Tramontina, R., Ciancaglini, I., Roman, E.K.B., Chacon, M.G., Correa, T.L.R., Dixon, N., Bugg, T.D.H., Squina, F.M., 2023. Sustainable biosynthetic pathways to value-added bioproducts from hydroxycinnamic acids. Appl. Microbiol. Biotechnol. 107, 4165–4185
- van Duuren, J., de Wild, P.J., Starck, S., Bradtmoller, C., Selzer, M., Mehlmann, K., Schneider, R., Kohlstedt, M., Poblete-Castro, I., Stolzenberger, J., Barton, N., Fritz, M., Scholl, S., Venus, J., Wittmann, C., 2020. Limited life cycle and cost assessment for the bioconversion of lignin-derived aromatics into adipic acid. Biotechnol. Bioeng, 117, 1381–1393.
- van Winden, W.A., Wittmann, C., Heinzle, E., Heijnen, J.J., 2002. Correcting mass isotopomer distributions for naturally occurring isotopes. Biotechnol. Bioeng. 80, 477, 479
- Varman, A.M., He, L., Follenfant, R., Wu, W., Wemmer, S., Wrobel, S.A., Tang, Y.J., Singh, S., 2016. Decoding how a soil bacterium extracts building blocks and metabolic energy from ligninolysis provides road map for lignin valorization. Proc. Natl. Acad. Sci. U. S. A. 113, E5802–E5811.
- Weiland, F., Barton, N., Kohlstedt, M., Becker, J., Wittmann, C., 2023. Systems metabolic engineering upgrades Corynebacterium glutamicum to high-efficiency cis, cismuconic acid production from lignin-based aromatics. Metab. Eng. 75, 153–169.
- Weiland, F., Kohlstedt, M., Wittmann, C., 2022. Guiding stars to the field of dreams: metabolically engineered pathways and microbial platforms for a sustainable lignin-based industry. Metab. Eng. 71, 13–41.

- Wendisch, V.F., de Graaf, A.A., Sahm, H., Eikmanns, B.J., 2000. Quantitative determination of metabolic fluxes during contilization of two carbon sources: comparative analyses with Corynebacterium glutamicum during growth on acetate and/or glucose. J. Bacteriol. 182, 3088–3096.
- Werner, A. Z., Cordell, W. T., Lahive, C. W., Klein, B. C., Singer, C. A., Tan, E. C. D., Ingraham, M. A., Ramirez, K. J., Kim, D. H., Pedersen, J. N., Johnson, C. W., Pfleger, B. F., Beckham, G. T., Salvachúa, D., Lignin conversion to β-ketoadipic acid by Pseudomonas putida via metabolic engineering and bioprocess development. Sci. Adv. 9, eadi0053.
- Wittmann, C., 2007. Fluxome analysis using GC-MS. Microb. Cell Fact. 6, 6.
 Wittmann, C., Heinzle, E., 2001. Application of MALDI-TOF MS to lysine-producing Corynebacterium glutamicum: a novel approach for metabolic flux analysis. Eur. J. Biochem. 268, 2441–2455.
- Wittmann, C., Heinzle, E., 2002. Genealogy profiling through strain improvement by using metabolic network analysis: metabolic flux genealogy of several generations of lysine-producing corynebacteria. Appl. Environ. Microbiol. 68, 5843–5859.
- Wittmann, C., Kiefer, P., Zelder, O., 2004a. Metabolic fluxes in Corynebacterium glutamicum during lysine production with sucrose as carbon source. Appl. Environ. Microbiol. 70, 7277–7287.
- Wittmann, C., Kim, H.M., Heinzle, E., 2004b. Metabolic network analysis of lysine producing *Corynebacterium glutamicum* at a miniaturized scale. Biotechnol. Bioeng. 87, 1–6.
- Wolf, M.E., Lalande, A.T., Newman, B.L., Bleem, A.C., Palumbo, C.T., Beckham, G.T., Eltis, L.D., 2024. The catabolism of lignin-derived p-methoxylated aromatic compounds by Rhodococcus jostii RHA1. Appl. Environ. Microbiol. 90 (23), e02155.
- Zhang, L., Larsson, A., Moldin, A., Edlund, U., 2022. Comparison of lignin distribution, structure, and morphology in wheat straw and wood. Ind. Crop. Prod. 187, 115432.
- Zhang, Y., Serate, J., Xie, D., Gajbhiye, S., Kulzer, P., Sanford, G., Russell, J.D., McGee, M., Foster, C., Coon, J.J., 2020. Production of hydrolysates from unmilled AFEX-pretreated switchgrass and comparative fermentation with Zymomonas mobilis. Bioresour. Technol. Rep. 11, 100517.